REPORT No. 42

THE THREE-DIMENSIONAL TURBULENT BOUNDARY LAYER IN A FREE VORTEX DIFFUSER

ERNEST B. GARDOW

January 1958

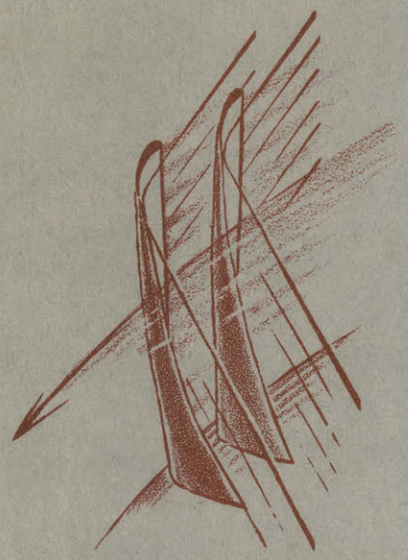

GAS TURBINE LABORATORY
MASSACHUSETTS INSTITUTE OF TECHNOLOGY
CAMBRIDGE · 39 · MASSACHUSETTS

THE THREE-DIMENSIONAL TURBULENT BOUNDARY LAYER IN A FREE VORTEX DIFFUSER

Ernest B. Gardow

Under the sponsorship of
Office of Naval Research
Contract Number: Nonr 1814(13)

Gas Turbine Laboratory

Report Number 42

January 1958

Massachusetts Institute of Technology

ACKNOWLEDGEMENTS

Many of the Gas Turbine Laboratory staff are to be thanked for lending their time to this effort.

Professors E. S. Taylor and A. H. Stenning, being supervisors of the project, continually had new ideas during the investigation. Mr. Warren Nelson was project leader for most of the duration of the study.

Mr. Toshio Kawasaki helped with the theoretical studies and Mr. Paul Cooper processed much of the data. Mr. Gabor Miskolczy is responsible for the design of the rotating screen.

Mr. Dalton Baugh and his staff are to be thanked for their help in the shop.

Mrs. Natalie Appleton and Mrs. Marna Reames are to be commended on the fine typing job.

ABSTRACT

Experimental velocity profiles and static pressure measurements were obtained from the flow in a free vortex diffuser. The purpose of the study was to obtain additional three dimensional boundary layer data and to compare it with existing theories. Free vortex diffuser behavior under varying inlet angles was also studied.

The boundary layer profiles correlated well with an existing model for three dimensional boundary layers generated by transverse pressure gradients. From this model boundary layer cross flow can be approximately predicted using a shearless flow analysis for the outer part of the boundary layer and an empirical correlation for the inner portion.

At high inlet swirl angles, a separation ring followed by reattachment was found in the diffuser.

Table of Contents

1 Introduction

The three-dimensional or skewed trubulent boundary layer problem has been attacked at the M.I.T. Gas Turbine Laboratory by studying the boundary layer in an apparatus using a jet of air impinging on a wall and in a free vortex or vaneless diffuser. Johnston (1) previously reported on the impinging jet configuration, and now this report will cover the results obtained from the diffuser experiment.

The study reported here is an extension and improvement of the work done by Isom (2). A modified form of the same apparatus was used.

The importance of studying three-dimensional flows is fairly evident. Most fluid machines, up to fairly recent times, have been designed from the vast storehouse of two-dimensional boundary layer theory and data. In order to improve the machines further, the three-dimensional characteristics of the boundary layer must be taken into consideration, because the flow in any fluid machine is rarely two-dimensional.

A free vortex diffuser was selected to study the skewed boundary layer, because it imposes an adverse pressure gradient on the flow and exhibits axial symmetry. The symmetry property simplifies the equations of motion, since all derivatives in the θ direction are zero. Axial symmetry also fixes the direction of the pressure gradient, which is in the radial direction.

The three-dimensional or skewed boundary layer is one in which the velocity vectors are not collateral, that is, not in one plane. Figure (1) gives a view of a typical three-dimensional boundary layer.

The skewed boundary layer is formed in the vaneless diffuser through the mechanism of secondary flow. The static pressure field is determined by the main stream flow outside the boundary layer and is a function

only of r . Neglecting viscous terms, the component of pressure gradient normal to a streamline is

$$\frac{\partial p}{\partial n} = \rho \frac{c^2}{R} \qquad (1.1)$$

where R is the radius of curvature of the streamline. For boundary layer fluid, the pressure gradient is the same, but C is less than the main stream velocity. Therefore, the radius of curvature of a boundary layer streamline must also be less than the radius of curvature of a main flow streamline, causing cross flows and skewing of the boundary layer.

2 Description of the Apparatus

A vaneless diffuser was selected for study of the three-dimensional boundary layer for reasons stated in the previous section. Study of the vaneless diffuser in itself is valuable, because no comprehensive evaluation of diffuser performance under various inlet swirl angles has been undertaken as far as the author knows.

Figure (2) shows the front wall of the diffuser removed. A screen in the form of an endless belt 83.75 inches in circumference and 2.55 inches wide is fastened to a rotating aluminum plate. Circulation is introduced into the flow by the cascade of screen wires which imparts tangential momentum to the air as it flows through the screen. This is contrasted with the approach of Isom (2) who used a circular cascade of stationary blades. This change was the essential difference between Isom's and the present study.

Figure (3) is a picture of the entire apparatus. Going from right to left are:

1.) The inlet filter bag made of a porous wool felt.

2.) A rubber inner tube used as a part of the faired inlet to the fan.

3.) The housing for the two-speed axial flow fan, which is capable of delivering air from 1800 to 8000 CFM.

4.) The bleed slot, which was used to vary the flow through the test section without stalling the fan.

5.) The settling chamber.

6.) The nozzle to direct the flow smoothly into the test section.

7.) The diffuser walls 2 inches apart.

Also shown is the hose used for boundary layer suction, along with the orifice plate and manometer for the suction flow measurement.

Figure (4) is a view of the front of the diffuser test section with the driving mechanism for the screen, consisting of a 2 horsepower AC motor, belts, and pulleys. The pulleys may be interchanged to vary the speed of the screen. A series of 11 ports were bored and reamed in a brass plate that was placed in the front wall of the diffuser. A three-hole cobra probe could be placed in any of the ports to measure the boundary layer on the back wall. Also illustrated are several rows of static pressure taps. In addition taps are located behind each of the probing ports. The three pressure transducers shown made it easy to obtain the various pressure measurements rapidly. The window was used for visual studies of the flow.

Figure (5) is a view of the three-hole cobra probe with micrometer screw for probing the boundary layer. The protracter was used to measure flow angles from the radial direction in the diffuser.

3 Development of the Apparatus

To obtain uniform velocities in the test section considerable development work on the apparatus was required. Isom (2) has mentioned in his paper that mailing tubes and screens were placed downstream of the

fan to smooth out the wake caused by the fan hub.

The rotating screen required a mesh that would allow a reasonable amount of flow into the test section. At the same time the screen would have to give the flow sufficient tangential momentum at a specific RPM to obtain a large inlet swirl angle. A screen of approximately 50% open area with wires from 0.008 to 0.015 inches in diameter was sought. After a few attempts at fabricating commercial stock screen into the desired circular shape, the W. S. Tyler Company, Cleveland, Ohio (a custom wire screen manufacturer) was consulted.

Two screen manufactured by this company were used in the apparatus.

Screen A	Screen B
30 x 30 mesh	33 x 14.5 mesh
0.0095" wire	0.014" wire
51% open area	42.8% open area

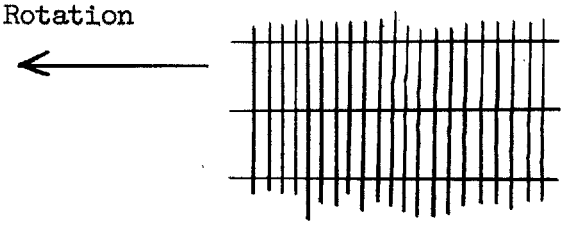

Both these screen were used in the experimental program. The most comprehensive data was taken with the screen B, since it gave a larger inlet swirl angle for a given RPM than did screen A.

A non-uniform velocity profile persisted in the region of flow outside the boundary layer despite the use of the high quality screen. Upon closer examination of the screen during operation, it was noticed that particles of dust and dirt had become lodged between the screen

wires. This suggested construction of the filter in front of the fan inlet. A large area filter was designed to minimize the pressure drop across the cloth.

With the addition of boundary layer suction from the slot in which the screen rode, the velocity profile became very uniform in the test section. Approximately 8% of the total flow was sucked off.

4 Experimental Methods

Figure (6) is a schematic diagram of the vaneless diffuser test section.

The program of experimentation consisted of taking boundary layer traverses at the various ports, starting with the first and continuing in the outward radial direction until the boundary layer had filled the passage. Table I is a tabulation of the location of the probing ports. The boundary layer velocity profiles were measured only on the back wall of the diffuser by reading stagnation pressure and static pressure against atmosphere on the pressure transducers, and by reading the angle of the velocity vector in the boundary layer with the protractor by nulling out the three-hole probe. As the probe approached the wall and the velocity gradient became steeper readings were taken at shorter intervals.

The angle ψ_i was varied by setting the through flow velocity of the fan at a constant value, and then rotating the screen at various RPM from 800 to 1410. The through flow velocity was measured by a pitot-static probe placed in the duct before the test section, and the rotational speed by focusing a stroboscopic light on the pulley attached to the shaft of the rotating plate. ψ_i ranged from 45° to 62.4° in the tests.

5 Summary of Isom's Work

Isom (2) in his experiment with the circular cascade of blades as the means of introducing swirl into the diffuser, came up with several interesting conclusions which will be mentioned here.

1.) Due to severe wakes shed from the blades of the cascade, the assumption of axial symmetry was not valid. The performance of the diffuser was poor, because the static pressure rise was small.

2.) The weak pressure gradient prohibited large cross flows in the boundary layer. A maximum skewing of only 9^{o} made Isom's experiment unsuitable for comprehensive three-dimensional boundary layer study. The present experiment obtained almost 45^{o} skewing.

3.) The correlation of the velocity profiles in the main stream or x-direction, using the "Law of the Wall" of Clauser (3) was quite successful. This implied the existence of a universal velocity distribution over a region for both two and three-dimensional boundary layers. Since then it has been concluded that for skewed flows of small cross flow, two-dimensional correlations hold with the cross flows not appreciably affecting the scatter of the data.

4.) Wall shear stress computed from Clauser's method and from the Karman shear stress law showed agreement within thirty to forty percent. Whether the discrepancies in the data resulted from ordinary scatter or from the effects of the slight three-dimensional flows could not be determined.

6 Discussion of Inlet Conditions

The performance of a vaneless diffuser depends greatly on the condition of the flow at the inlet. It was proved in Isom's experiment that the wakes shed from stationary objects in adverse pressure gradients persist and thicken. These caused unsymmetric pressure and velocity distributions in the diffuser.

In an attempt to correct the flow, the rotating screen was installed. It was hoped that the small wakes shed from the cascade of screen wires would mix out in a short distance. This proved to be the case. From a set of readings of the static pressure taps all around the diffuser, it seemed that the flow was symmetric.

It was later proposed by Senoo (4) that wakes shed from moving objects mix out in a short distance. With no pressure discontinuities recorded, it was assumed that there were no severe wakes present.

The overall performance of the diffuser was high, as proved by data given later in this report. The outlet conditions from the rotating screen used in the apparatus were much more uniform than conditions from any centrifugal compressor impeller, thereby resulting in a more efficient vaneless diffuser.

7 Presentation of Pressure Coefficient Data

The behavior of the apparatus as an actual diffuser was studied. If there were a definite functional relationship between inlet swirl angle and diffuser pressure coefficient, diffuser performance could be predicted over the whole range of operation.

It was found that as ψ_i was increased, by increasing the speed of the screen,

P.C. decreased, where

$$P.C. = \frac{P_e - P_i}{\frac{1}{2}\rho C_i^2} \tag{7.1}$$

For this diffuser geometry the maximum theoretical P.C. = 0.813. Figure (7) illustrates how P.C. varied with ψ_i, the data points being the ones obtained for each of the eight runs.

Let it now be assumed that the pressure coefficient depends only on the inlet angle ψ_i according to the functional relationship shown in Figure (7). An optimum ψ_i for the best diffuser performance may now be determined.

From Figure (6) it can be seen that

$$C_{ri} = C_{\theta i} \cot \psi_i \tag{7.2}$$

also from Bernoulli's equation

$$P_{oi} = P_i + \rho/2 \left(C_{ri}^2 + C_{\theta i}^2\right) \tag{7.3}$$

The pressure at the exit of the diffuser depends on P.C.

$$P_e = P_i + (P.C.)\frac{\rho}{2}\left(C_{\theta i}^2 + C_{ri}^2\right) \tag{7.4}$$

Substituting (2) and (3) in (4)

$$P_e = P_{oi} + \frac{\rho}{2}(P.C. - 1) C_{\theta i}^2 \left(1 + \cot^2 \psi_i\right) \tag{7.5}$$

Rearranging

$$\frac{P_e}{\frac{1}{2}\rho C_{\theta i}^2} = \frac{P_{oi}}{\frac{1}{2}\rho C_{\theta i}^2} - \underbrace{(1 - P.C.)}_{(a)} \underbrace{\left(1 + \cot^2 \psi_i\right)}_{(b)} \tag{7.6}$$

If we are given a centrifugal impeller with fixed values of tangential velocity, C_{ei}, and stagnation pressure leaving the impeller, P_{oi}, the designer of the vaneless diffuser can select a value of ψ_i that will give a maximum exit pressure, p_e. ψ_i is determined by fixing the distance between the diffuser walls.

P_e is at its maximum when the function (a) (b) in equation (6) is a minimum. P.C. decreases as ψ_i decreases, therefore function (a) will increase. But function (b) will decrease in value at a greater rate than (a) increases. Therefore, there will be a value of ψ_i where (a) (b) is a minimum.

By extrapolating the P.C. versus ψ_i curve from our experiment, Figure (7), p_e is a maximum when $\psi_i = 74°$.

8 Presentation of Boundary Layer Data

A considerable quantity of three-dimensional boundary layer information was obtained from the apparatus. Boundary layer and pressure distribution data was compiled for seven runs. An eighth run was also tabulated, in which only pressure distribution was read. The boundary layer had filled the passage after the first port so no traverses were taken.

Each of the traverses is designated by a number as shown by the following example.

A - 45.2 - 1

The letter stands for the screen used. The first number stands for the angle ψ_i, which is the most significant variable for all the runs. The second number stands for the port in which the traverse was taken.

Table II is a tabulation of the flow conditions for each of the complete runs. It includes ψ_i, screen rotational speed needed to

obtain this ψ_i, and the flow rate in the test section. (Boundary layer suction flow rate has been subtracted to obtain this figure.)

The general equations for three-dimensional boundary layers are most useful when expressed in streamline coordinates. Referring to Figure (1), one may define the direction of the velocity vector just outside the boundary layer as the x-direction with its magnitude being U. In the boundary layer, components of velocity in the x-direction are called u. Components of velocity in the z-direction perpendicular to x are designated w. Velocity components v, normal to the wall in the y direction, are neglected. Table III is a tabulation of the experimental velocity traverse data. For each value of y there is value of u/U and w/U. All velocity components are normalized with respect to the main flow streamline velocity. Figure (8) illustrates two samples of the velocity profiles.

The boundary layer equations in three-dimensions are usually expressed in their integrated form, called the momentum integral equations. Johnston (1) has derived these equations, defining the momentum integral quantities in streamline coordinates. These boundary layer equations along with several auxiliary equations are the tools available to solve any turbulent boundary layer problem. They are repeated here.

$$\frac{\partial \theta_x}{\partial x} + \frac{\partial \theta_{xz}}{\partial z} + 2(\theta_x + \delta_x)\frac{1}{U}\frac{\partial U}{\partial x} + \frac{1}{U}\frac{\partial \bar{W}}{\partial z}(\theta_x + \theta_z) = \frac{\tau_{ox}}{\rho U^2} \qquad (8.1)$$

and

$$\frac{\partial \theta_z}{\partial z} + \frac{\partial \theta_{zx}}{\partial x} + (\theta_z - \theta_x - \delta_x)\frac{1}{U}\frac{\partial U}{\partial z} + 2\theta_{zx}\left[\frac{1}{U}\frac{\partial U}{\partial x} + \frac{1}{U}\frac{\partial \bar{W}}{\partial z}\right] = \frac{-\tau_{oz}}{\rho U^2} \qquad (8.2)$$

$\frac{\partial \overline{W}}{\partial z}$ is a term involving the streamline divergence or convergence in the main stream. The definitions of the integral quantities are:

$$\delta_x = \int_0^\infty \left(1 - \frac{u}{U}\right) dy \tag{8.3}$$

$$\theta_x = \int_0^\infty \left(1 - \frac{u}{U}\right) \frac{u}{U}\, dy \tag{8.4}$$

$$\theta_{xz} = \int_0^\infty \left(1 - \frac{u}{U}\right) \frac{w}{U}\, dy \tag{8.5}$$

$$\delta_z = \int_0^\infty \frac{w}{U}\, dy \tag{8.6}$$

$$\theta_z = \int_0^\infty \left(\frac{w}{U}\right)^2 dy \tag{8.7}$$

$$\theta_{zx} = \int_0^\infty \frac{u}{U} \frac{w}{U}\, dy \tag{8.8}$$

$$H_x = \frac{\delta_x}{\theta_x} \tag{8.9}$$

where y is the distance from the wall. H_x is known as the shape factor.

These integral quantities have been obtained by graphical integration of the velocity profiles for all the runs. Table IV is a tabulation of these quantities.

9 Representation of the Boundary Layer by a Polar Plot

Johnston (1) has given an historical sketch of various models of three-dimensional boundary layers as proposed by several authors. However, he found that the best model was one in which cross flow velocity was related to the main flow component of velocity. This was done by plotting the data in a velocity polar plot. Figure (9) is a sketch of the plot showing the significant parameters. The model breaks up the flow into two regions, divided at $\left(\frac{w}{U}\right)_p$. In the region (1) near the wall $\frac{w}{U} = \epsilon \frac{u}{U}$ and in the region (2) near the main flow $\frac{w}{U} = A\left(1 - \frac{u}{U}\right)$.

Figures (10a) and (10b) are samples of the experimental profiles. The other traverses not shown gave similar polar plots, so for the three-dimensional boundary layers generated by transverse pressure gradients investigated up to this point the velocity polar model seems valid. The points fall on two straight lines except near the peak where they round off. The velocity traverses obtained in the vaneless diffuser gave more points in the region (1) close to the wall than any of the profiles investigated by Johnston (1).

Table V is a tabulation of the parameters of the polar plots along with the other significant variables for each traverse. It includes A, ϵ, U, ψ, β_w, γ_w, C_f, and $p_s - p_a$. The assumption of logarithmic spiral flow does not hold for this vaneless diffuser, since α decreases with increasing r. This results from the growth of the boundary layer causing greater radial velocity, C_r.

10 Correlation of Outer Portion of the Boundary Layer

The outer portion of the boundary layer or region (2) can be analysed very simply, if we assume that it is a region where friction can be largely neglected. This can be done because the friction forces act mainly in the region (1) close to the wall.

Johnston (1) arrived at an expression for the parameter A by linearizing the momentum equations. The same expression may be obtained by applying secondary flow theory as will be done here.

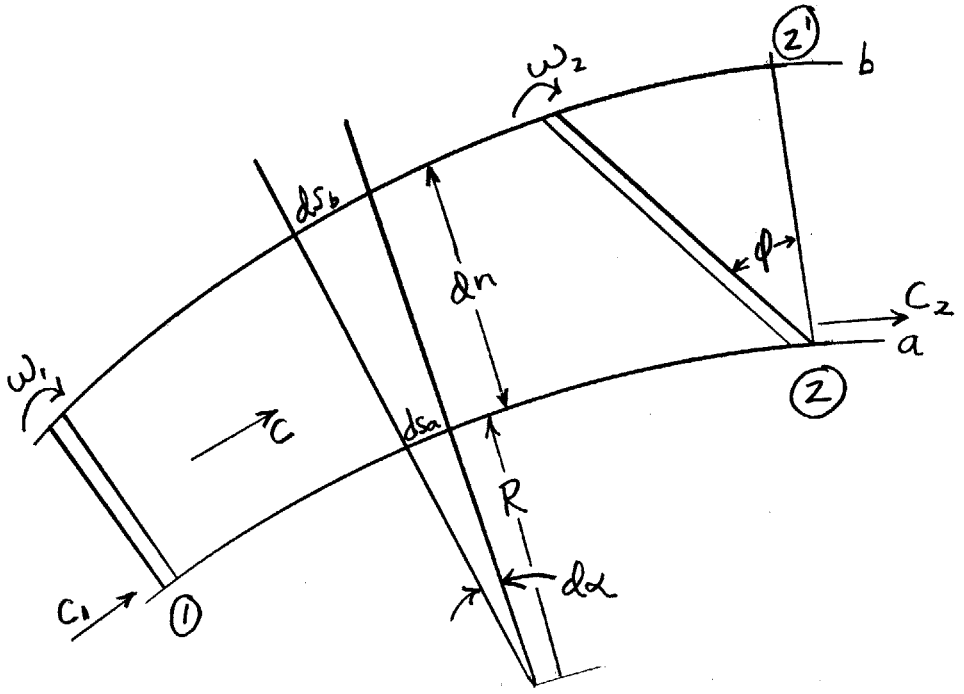

The above figure indicates two stramlines a and b. ω_1 and ω_2 are the vorticity 1 and 2. No vorticity is generated or dissipated between 1 and 2.

The time it takes for fluid to go from 1 to 2 along a and b is

$$t = \int_{1\,a}^{2} \frac{ds}{c} = \int_{1\,b}^{2} \frac{ds}{c} \qquad (10.1)$$

but
$$\int_{1b}^{2} \frac{ds}{c} = \int_{1b}^{2'} \frac{ds}{c} - \int_{2b}^{2'} \frac{ds}{c} \tag{10.2}$$

therefore
$$\int_{2b}^{2'} \frac{ds}{c} = \int_{1b}^{2'} \frac{ds}{c} - \int_{1a}^{2} \frac{ds}{c} \tag{10.3}$$

The pressure gradient normal to the streamlines is

$$\frac{\partial p}{\partial n} = \rho \frac{c^2}{R} \tag{10.4}$$

Differentiating Bernoulli's equation with respect to a change in the normal direction to streamline in a Bernoulli surface gives:

$$\frac{dp}{\partial n} = -\rho c \frac{\partial c}{\partial n} \tag{10.5}$$

Therefore
$$\frac{\partial c}{\partial n} = -\frac{c}{R} \tag{10.6}$$

For a change of $d\alpha$ in α

$$\frac{ds_b}{ds_a} = \frac{R + dn}{R} \tag{10.7}$$

where ds is an increment along a streamline and dn the distance between the streamlines.

C at any point a distance dn away from streamline a is C_b, or

$$C_b = C_a + \frac{\partial c}{\partial n} dn \tag{10.8}$$

Therefore

$$C_b = C_a - \frac{C_a}{R}\, dn \tag{10.9}$$

Also from (7)

$$ds_b = ds_a\left(1 + \frac{dn}{R}\right) \tag{10.10}$$

Relating the terms in equation (3) to the streamline a

$$\int_{2b}^{2'} \frac{ds}{c} = \int_{1a}^{2} \frac{\left(1 + \frac{dn}{R}\right) ds}{C\left(1 - \frac{dn}{R}\right)} - \int_{1a}^{2} \frac{ds}{c} \tag{10.11}$$

Multiplying the second integral by $1 + \frac{dn}{R}$ and neglecting second order terms gives:

$$\int_{2b}^{2'} \frac{ds}{C} = \int_{1a}^{2} \left(1 + 2\,\frac{dn}{R}\right) \frac{ds}{C} - \int_{1a}^{2} \frac{ds}{C} \tag{10.12}$$

Therefore

$$\int_{2b}^{2'} \frac{ds}{C} = 2 \int_{1a}^{2} \frac{dn}{R}\, \frac{ds}{C} \tag{10.13}$$

or

$$\frac{dn_2 \tan\phi}{C_2} = 2 \int_{1}^{2} \frac{dn}{C R}\, ds \tag{10.14}$$

From continuity

$$C_1 \, dn_1 = C_2 \, dn_2 = C \, dn \tag{10.15}$$

so

$$\frac{C_2 \, dn_2 \tan\phi}{C_2^2} = 2 C_1 \, dn_1 \int_1^2 \frac{ds}{c^2 R} \tag{10.16}$$

or

$$\frac{\tan\phi}{C_2^2} = 2 \int_1^2 \frac{d\alpha}{c^2} \tag{10.17}$$

The vorticity components normal and tangential to the streamlines at 2 are

$$\omega_2 \cos\phi = \frac{du}{dy} \tag{10.18}$$

$$\omega_2 \sin\phi = \frac{dv}{dy} \tag{10.19}$$

where y is the direction perpendicular to the Bernoulli surfaces and perpendicular to the wall. Eliminate ω_2 from (18) and (19)

$$\frac{dv}{dy} = \frac{du}{dy} \tan\phi \tag{10.20}$$

Integrate

$$\int_y^\delta \frac{dv}{dy} dy = \int_y^\delta \tan\phi \, \frac{du}{dy} dy \tag{10.21}$$

Changing limits of integration, we get

$$\int_{w}^{0} dw = \int_{u}^{U} \tan\phi \, du \tag{10.22}$$

$$-w = (U-u)\tan\phi \tag{10.23}$$

$$\tan\phi = \frac{-w}{U-u} = A \tag{10.24}$$

Since U = C at the edge of the boundary layer.

$$A = -2U_2^2 \int_1^2 \frac{d\alpha}{U^2} \tag{10.25}$$

If we start with a collateral boundary layer where $\alpha = 0$

$$A = -2U_\alpha^2 \int_0^\alpha \frac{d\alpha}{U^2} \tag{10.26}$$

This is the same expression as the one obtained by Johnston (1). The integration is carried out along the streamline.

For the vaneless diffuser the previous equation may be written as

$$A = -2U_r^2 \int_{r_i}^{r} \frac{1}{U^2} \frac{d\alpha}{dr} dr \tag{10.27}$$

where $A = \alpha = 0$ at r_i. It can be shown that along a main flow streamline (assumed to be a log spiral for simplicity) the quantity

$$\frac{d\alpha}{dr} = -\frac{\tan\psi}{r} \tag{10.28}$$

See Figure (11).

The continuity equation and conservation of angular momentum state that

$$rC = r_i C_i \tag{10.29}$$

Therefore

$$A = -\frac{2}{r^2}\int_{r_i}^{r} r^2\left(-\frac{\tan\psi}{r}\right)dr \tag{10.30}$$

$$A = \tan\psi\left[1 - \left(\frac{r_i}{r}\right)^2\right] \tag{10.31}$$

Since ψ is a constant for log spiral flow, A is a function of radial position in the diffuser for a given inlet ψ.

The theoretical A has been plotted versus $1 - \left(\frac{r_i}{r}\right)^2$ for two values of ψ_i, also the actual experimental values of A have been plotted for these ψ_i's. Figure (12) illustrates these correlations.

The experimental values always fall short of the theoretical values determined by secondary flow theory. The theory states that when a flow with a stagnation pressure gradient is turned in a bend a component of the vorticity is produced along the streamline. This vorticity will determine the amount of cross flow in the boundary layer, thereby fixing a value of the parameter A.

In the present study vorticity was built up as the flow was being turned in the bend. The boundary layer was sucked off to begin with, so any secondary flow that developed had to result from vorticity built up as it was turned. It would naturally be expected then that the experimental cross flow would not be as great as the theoretical values.

However, the observed values are never less than 70% to 80% of the theoretical values, so there seems to be some value in the correlation. Perhaps a modified secondary flow theory, taking into account generated vorticity, could predict A to a greater degree of accuracy.

11 The Inner Portion of the Boundary Layer

Having determined A, if the peak of the velocity polar plot could be determined, the boundary layer cross flow would be pinned down. Johnston (1) did this by assuming the peak was fairly near the edge of the laminar sublayer. However, when this was tried with the data of the present study, it was found that the Reynolds number, was too high for the peak to be at the edge of the laminar sublayer, and in fact, the peak appeared to be in the region of high turbulence.

If, however, a dimensionless value is defined,

$$u_p^* = \frac{u_p}{\sqrt{\tau_{ox}/\rho}} \tag{11.1}$$

a useful correlation results.

From the geometry of the polar plot

$$\left(\frac{w}{U}\right)_p = \epsilon \left(\frac{u}{U}\right)_p = A\left[1 - \left(\frac{u}{U}\right)_p\right] \tag{11.2}$$

Solving for $\left(\frac{u}{U}\right)_p$

$$\left(\frac{u}{U}\right)_p = \frac{1}{1 + \epsilon/A} \tag{11.3}$$

Divide both sides by $\sqrt{\tau_{ox}/\rho}$

$$\frac{u_p}{\sqrt{\tau_{ox}/\rho}} = \frac{U}{\sqrt{\frac{\tau_{ox}}{\rho}}\left[1 + \frac{\epsilon}{A}\right]} \tag{11.4}$$

$$\tau_{ox} = \tfrac{1}{2}\rho U^2 C_{fx} \tag{11.5}$$

Therefore $$u_p^* = \frac{1}{\left(1+\frac{\epsilon}{A}\right)\sqrt{\frac{1}{2}C_{fx}}} \qquad (11.6)$$

but $$C_{fx} = \frac{C_f}{\sqrt{1+\epsilon^2}} \qquad (11.7)$$

$$u_p^* = \frac{1}{\left(1+\frac{\epsilon}{A}\right)\sqrt{\frac{C_f}{2}\frac{1}{\sqrt{1+\epsilon^2}}}} \qquad (11.8)$$

or

$$\left(1+\frac{\epsilon}{A}\right)u_p^* = \frac{\sqrt[4]{1+\epsilon^2}}{\sqrt{\frac{C_f}{2}}} \qquad (11.9)$$

From the profiles of present study, as well as those of Johnston (1), Gruschwitz (5), and Keuthe, et al. (6), $\frac{\epsilon}{A}+1$ was determined from the geometry of the polar plot. C_f was determined from Clauser's "Law of the Wall", as modified by Johnston (1). Figure (13) indicates that u^*_p correlates as a constant equal to 14 with a scatter of approximately 25%.

If skin friction can somehow be determined, a value of u_p is fixed and the peak of the velocity polar plot is determined. Skin friction can be determined to the same degree of accuracy as the scatter of the u^*_p correlation by modifications of several two-dimensional theories.

The cross flow at any point in the boundary layer and the parameter ϵ are now determined for all cases.

In the present study other correlations of a velocity divided by shear velocity were tried. Johnston (1) used the absolute velocity at the peak, c_p, divided by the absolute shear velocity. Although it is not certain whether u^*_p or c^*_p is the parameter to fix, it does seem that a correlation of this type will be used to predict cross flow profiles in the future.

12 Total Overturn Angle as a Function of Inlet Swirl Angle

In an attempt to find other consistent behavior in the diffuser, it was decided to plot ψ_i versus the maximum γ_w obtained at any of the ports in the diffuser.

Figure (14) shows this correlation for each of the runs. The line of $(\gamma_w)_{MAX}/\psi_i = \frac{1}{2}$ is shown and fits most of the data. This may give the designer of a vaneless diffuser some idea of what the boundary layer will do when the inlet swirl angle is varied. If the inlet swirl angle is 60° the boundary layer limiting wall streamline will go approximately in the tangential direction. Whether the upturn of the data for $\psi_i > 60^\circ$ is significant is not known, because a higher ψ_i than 62° could not be obtained with the present apparatus.

13 Discussion of Separation in the Diffuser

If the angle ψ_i is greater than 60° there is a region where the wall streamlines and those close to the wall pass through the tangential direction and make an angle greater than 90° with the outward radius vector. Such conditions have been attained as proved by Figure (14). When ψ_i was 62°, the limiting wall streamline angle $\beta_w = 96^\circ$.

This is a type of separation in three-dimensions proposed by Johnston (7) and is illustrated in Figure (15). This shows the components of velocity in the radial direction. In midstream the radial velocity is fairly substantial until it diminishes to zero close to the wall, and from that point to the wall there is a back flow. In order to maintain continuity the back flowing fluid must recirculate as shown in the illustration. This type of separation has been designated as a bubble by Maskell (8).

Figure (16) shows the direction of the limiting wall streamlines. This has also been discussed by Maskell (8). The lines of separation and detachment are the extent of the bubble.

Measurements of direction with the three-hole cobra probe on one side of the test section, and visualization of smoke injected into the other side of the test section indicated that the flow was reasonably axisymmetric. If the condition holds the bubble would extend around the center of the diffuser in the form of a ring. The streamlines would then spiral around in the ring.

Figure (7) indicated a loss in diffuser pressure coefficient as ψ_i was increased. Whether part or all of the increase in loss for $\psi_i > 60$ could be attributed to the formation of the separation bubble could not be determined. There was no indication that the separated region shed downstream. The flow always reattached to the wall in the tests made with this condition. This was quite unexpected here because of the high adverse pressure gradient.

Figure (17) is a plot of static pressure distribution for run B-59.6. There is a deviation from the expected curve just at the position in the diffuser where the back flow is most severe. This indicates that the pressure rise was less, as a result of the separation ring. However, further out in the diffuser the static pressure data jumps back into the smooth curve clearly proving that the flow reattached itself with better diffusion resulting.

14 Conclusions

The following conclusions concerning the diffuser and the boundary layer can be stated.

1.) The designer of a vaneless diffuser can design for a maximum value of exit pressure, p_e. This involves fixing the inlet angle ψ_i at its optimum value for a given cetrifugal impeller with a fixed p_{oi} and $c_{\Theta i}$.

2.) The method of expressing three-dimensional boundary layer cross flow as a function of its main flow component, which has been proposed by Johnston, is sound. It is remarkable that two entirely different experiments with the three-dimensional turbulent boundary layer can be correlated using the same velocity polar model.

3.) The polar plot can be broken into two regions assuming that the tips of the velocity vectors fall along the two straight lines. The outer region parameter A can be approximately determined using a simple shearless theory of secondary flow. The inner region parameter ϵ can be determined by fixing the position of the polar plot peak. This involves the determination of skin friction in the main flow direction.

4.) Obtaining cross flows such that steady flow separation in three-dimensions occurs, makes the vaneless diffuser a useful piece of apparatus for separation studies.

List of Symbols

A	a model parameter
c	velocity
c^*_p	dimensionless quantity; absolute velocity at model peak divided by absolute friction velocity
$H_x = \frac{\delta_x}{\theta_x}$	shape factor
n	direction normal to streamline
p	pressure
p_o	stagnation pressure
p_s	static pressure
p_a	atmospheric pressure
P.C.	pressure coefficient
R	radius of curvature of streamline
r	radius in the diffuser
s	direction along streamline
t	time
u,v,w	velocity components in boundary layer (see Figure 1)
u^*_p	dimensionless quantity, component of velocity in main flow direction a model peak divided by component of friction velocity
u^*	friction velocity
U	absolute velocity at edge of the boundary layer
$\frac{\partial \overline{w}}{\partial z}$	term involving divergence of streamlines in momentum integral equations
x,y,z	streamline coordinate system (see Figure 1)
α	streamline turning angle
β	angle that a boundary layer vector makes with the radial direction

γ_w	angle between wall shear stress vector and main flow direction
$\left\{\begin{matrix}\delta_x, \delta_z, \Theta_x \\ \Theta_z, \Theta_{xz}, \Theta_{zx}\end{matrix}\right\}$	momentum thickness quantities (see Equations 8-3 to 8-8)
$\epsilon = \tan \gamma_w$	a model parameter
ν	kinematic viscosity
ϕ	vorticity angle
ρ	mass density
τ_o	wall shearing stress
ψ	angle between main flow direction and radial direction
ω	vorticity

Subscripts

a,b	streamline designation
e	exit of diffuser
i	inlet of diffuser
r	radial direction
p	refers to conditions at peak of velocity polar plot model
w	refers to conditions at the wall
θ	tangential direction

References

1. Johnston, J. P., "Three-Dimensional Turbulent Boundary Layer", M.I.T. Gas Turbine Laboratory, Report No. 39, May 1957.

2. Isom, Morris P., "The Three-Dimensional Boundary Layer in a Vaneless Diffuser", S.M. Thesis, M.I.T. Department of Electrical Engineering, May 1956.

3. Clauser, Francis H., "Turbulent Boundary Layers in Adverse Pressure Gradients", Journal of the Aeronautical Sciences, Vol. 21, No. 2, February 1954.

4. Senoo, Yasutoshi, "Personal Communication".

5. Gruschwitz, E., "Turbulente Reibungsschichten mit Sekundärströmmung", Ingenieur Archiv., Bd. VI, 1935, S. 355-365.

6. Keuthe, A. M., McKee, P. B., Curry, W. H., "Measurements in the Boundary Layer of a Yawed Elliptical Wing", NACA TN 1946, September 1949.

7. Johnston, J. P., "Experimental Data on Three-Dimensional Flow in a Centrifugal Compressor Diffuser", M.I.T. Gas Turbine Laboratory, Report No. 27-7, December 1954.

8. Maskell, E. C., "Flow Separation in Three-Dimensions", Report No. Aero 2565, Royal Aircraft Establishment, Farnborough, November 1955.

TABLE I

Diffuser Geometry

Outer radius (re) of diffuser = 39 inches.
Distance between diffuser walls = 2 inches.

Screen r/re = 0.342

Port No.	r/re
1	0.433
2	0.489
3	0.542
4	0.593
5	0.649
6	0.692
7	0.744
8	0.796
9	0.846
10	0.899
11	0.952
exit	1.000

ADDENDA

Reference for derivation in Section 10.

Otsuka, Shintaro,
"A Note About Secondary Circulation in Two-Dimensional Flow", Journal of the Japanese Society of Aeronautical Engineering, Vol. 2-8, August 1954, pp. 191-192 (in Japanese).

TABLE II

Flow Data

Run	ψ_i	Screen Speed (RPM)	Q (CFM)
A-45.2	45.2°	900	2135
A-51.6	51.6°	1000	2145
B-50.6	50.6°	800	2070
B-52.1	52.1°	900	2050
B-54.5	54.5°	1000	1980
B-59.0	59.0°	1275	2315
B-59.6	59.6°	1410	2315
B-62.4	62.4°	1410	2245

TABLE III

A-45.2-1

Y(in.)	$\frac{u}{U}$	$\frac{w}{U}$
0.204	1.000	0.000
0.154	0.990	0.009
0.129	0.968	0.022
0.104	0.926	0.029
0.084	0.896	0.042
0.064	0.836	0.055
0.054	0.774	0.058
0.044	0.759	0.065
0.034	0.726	0.067
0.026	0.671	0.071
0.021	0.638	0.074
0.016	0.604	0.074
0.011	0.520	0.064
0.008	0.433	0.053

A-45.2-2

Y(in.)	$\frac{u}{U}$	$\frac{w}{U}$
0.318	1.000	0.000
0.268	0.995	0.000
0.218	0.953	0.013
0.198	0.940	0.022
0.178	0.917	0.034
0.158	0.891	0.042
0.148	0.854	0.051
0.178	0.818	0.067
0.108	0.808	0.072
0.098	0.789	0.073
0.088	0.751	0.080
0.078	0.742	0.087
0.068	0.716	0.090
0.058	0.711	0.098
0.048	0.690	0.108
0.038	0.644	0.106
0.028	0.596	0.106
0.020	0.539	0.105
0.015	0.512	0.110
0.010	0.447	0.096
0.008	0.436	0.093

A-45.2-3

Y(in.)	$\frac{u}{U}$	$\frac{w}{U}$
0.516	1.000	0.000
0.416	0.996	0,000
0.366	0.958	0.010
0.316	0.940	0.026
0.266	0.880	0,046
0.241	0.847	0.058
0.216	0.811	0.071
0.196	0.792	0.078
0.176	0.769	0.089
0.156	0.756	0.099
0.136	0.702	0.102
0.116	0.667	0.110
0.096	0.649	0.119
0.086	0.638	0.123
0.076	0.604	0.124
0.066	0.569	0.124
0.056	0.577	0.134
0.046	0.561	0.133
0.036	0.527	0.130
0.028	0.487	0.123
0.023	0.450	0.110
0.018	0.338	0.083
0.013	0.253	0.064
0.008	0.126	0.032

A-45.2-4

Y(in.)	$\frac{u}{U}$	$\frac{w}{U}$
0.626	1.000	0.000
0.526	0.988	0.007
0.476	0.986	0.009
0.426	0.947	0.025
0.376	0.927	0.035
0.326	0.901	0.060
0.276	0.844	0.084
0.226	0.785	0.104
0.206	0.756	0.106
0.186	0.742	0.117
0.166	0.711	0.124
0.146	0.653	0.122
0.126	0.644	0.131
0.116	0.639	0.141
0.106	0.648	0.145
0.096	0.622	0.148
0.086	0.616	0.154
0.076	0.589	0.153
0.066	0.567	0.153
0.056	0.521	0.149
0.046	0.535	0.160
0.036	0.497	0.153
0.028	0.440	0.140
0.023	0.388	0.126
0.018	0.365	0.120
0.013	0.293	0.096
0.008	0.197	0.065

TABLE III (contd.)

A-45.2-5			A-45.2-6			A-45.2-7		
Y(in.)	$\frac{u}{U}$	$\frac{w}{U}$	Y(in.)	$\frac{u}{U}$	$\frac{w}{U}$	Y(in.)	$\frac{u}{U}$	$\frac{w}{U}$
0.735	1.000	0.000	0.732	1.000	0.000	0.848	1.000	0.000
0.635	0.982	0.003	0.632	0.952	0.013	0.798	0.996	0.005
0.535	0.956	0.022	0.582	0.923	0.035	0.748	0.976	0.014
0.485	0.913	0.034	0.532	0.901	0.047	0.698	0.963	0.027
0.435	0.880	0.049	0.482	0.882	0.062	0.648	0.933	0.039
0.385	0.872	0.074	0.432	0.846	0.077	0.598	0.897	0.047
0.335	0.774	0.086	0.407	0.812	0.082	0.548	0.873	0.064
0.285	0.723	0.104	0.382	0.806	0.097	0.498	0.828	0.082
0.235	0.688	0.124	0.357	0.782	0.106	0.448	0.794	0.092
0.215	0.679	0.134	0.332	0.758	0.115	0.398	0.765	0.113
0.195	0.670	0.137	0.307	0.741	0.126	0.348	0.725	0.121
0.175	0.648	0.145	0.282	0.687	0.125	0.323	0.691	0.127
0.155	0.647	0.151	0.257	0.683	0.142	0.298	0.702	0.140
0.135	0.633	0.160	0.232	0.682	0.147	0.273	0.644	0.136
0.125	0.622	0.167	0.212	0.664	0.155	0.248	0.651	0.154
0.115	0.580	0.160	0.192	0.635	0.160	0.228	0.629	0.155
0.105	0.586	0.169	0.172	0.598	0.158	0.208	0.634	0.163
0.095	0.566	0.174	0.152	0.582	0.161	0.188	0.609	0.168
0.085	0.548	0.173	0.132	0.546	0.159	0.168	0.565	0.166
0.075	0.560	0.180	0.122	0.549	0.169	0.148	0.574	0.173
0.065	0.514	0.172	0.112	0.565	0.182	0.128	0.511	0.160
0.055	0.477	0.165	0.102	0.545	0.179	0.108	0.532	0.175
0.045	0.490	0.174	0.092	0.538	0.187	0.098	0.518	0.179
0.037	0.464	0.170	0.082	0.532	0.187	0.088	0.506	0.177
0.032	0.449	0.167	0.072	0.498	0.184	0.078	0.485	0.178
0.027	0.361	0.134	0.062	0.493	0.183	0.068	0.471	0.176
0.022	0.361	0.134	0.052	0.480	0.186	0.058	0.465	0.175
0.017	0.320	0.120	0.042	0.463	0.180	0.048	0.444	0.174
0.012	0.314	0.118	0.034	0.435	0.169	0.038	0.430	0.169
0.008	0.255	0.096	0.029	0.417	0.162	0.028	0.395	0.155
			0.024	0.404	0.157	0.020	0.348	0.137
			0.019	0.286	0.111	0.015	0.313	0.123
			0.014	0.226	0.088	0.010	0.251	0.099
			0.008	0.174	0.068	0.008	0.241	0.095

TABLE III (contd.)

A-45.2-8			A-45.2-9			A-51.6-1		
Y(in.)	$\frac{u}{U}$	$\frac{w}{U}$	Y(in.)	$\frac{u}{U}$	$\frac{w}{U}$	Y(in.)	$\frac{u}{U}$	$\frac{w}{U}$
0.991	1.000	0.000	1.008	1.000	0.000	0.190	1.000	0.000
0.941	0.990	0.007	0.983	0.989	0.000	0.180	1.000	0.003
0.891	0.960	0.023	0.958	0.985	0.010	0.170	0.998	0.003
0.841	0.934	0.028	0.908	0.954	0.018	0.160	0.990	0.009
0.791	0.918	0.043	0.858	0.926	0.035	0.150	0.984	0.014
0.741	0.878	0.054	0.808	0.910	0.046	0.140	0.973	0.018
0.691	0.853	0.066	0.758	0.880	0.060	0.130	0.958	0.023
0.641	0.827	0.084	0.708	0.849	0.072	0.120	0.944	0.028
0.591	0.795	0.094	0.658	0.826	0.080	0.110	0.926	0.034
0.541	0.767	0.106	0.608	0.796	0.094	0.100	0.908	0.040
0.491	0.740	0.125	0.558	0.772	0.110	0.090	0.884	0.045
0.466	0.720	0.132	0.508	0.745	0.123	0.080	0.858	0.051
0.441	0.699	0.135	0.483	0.744	0.131	0.070	0.832	0.057
0.416	0.687	0.143	0.458	0.723	0.134	0.060	0.793	0.062
0.391	0.676	0.149	0.433	0.706	0.143	0.050	0.748	0.071
0.366	0.669	0.158	0.408	0.695	0.146	0.045	0.717	0.080
0.341	0.660	0.172	0.383	0.682	0.154	0.040	0.696	0.088
0.316	0.638	0.175	0.358	0.669	0.158	0.035	0.674	0.093
0.291	0.628	0.188	0.333	0.658	0.165	0.030	0.640	0.097
0.266	0.616	0.187	0.308	0.633	0.171	0.025	0.615	0.102
0.241	0.604	0.195	0.283	0.625	0.179	0.020	0.587	0.104
0.216	0.583	0.200	0.258	0.607	0.176	0.017	0.575	0.102
0.191	0.575	0.207	0.233	0.585	0.188	0.012	0.519	0.092
0.171	0.555	0.210	0.208	0.582	0.200	0.010	0.490	0.086
0.151	0.540	0.216	0.188	0.573	0.204	0.008	0.472	0.083
0.131	0.520	0.216	0.168	0.571	0.209			
0.111	0.503	0.222	0.148	0.553	0.204			
0.091	0.491	0.220	0.128	0.531	0.210			
0.071	0.464	0.214	0.108	0.514	0.218			
0.061	0.462	0.218	0.880	0.510	0.226			
0.051	0.425	0.210	0.078	0.494	0.228			
0.041	0.418	0.209	0.068	0.489	0.225			
0.031	0.396	0.201	0.058	0.476	0.220			
0.023	0.335	0.170	0.048	0.462	0.213			
0.013	0.281	0.142	0.038	0.432	0.210			
0.008	0.211	0.107	0.030	0.381	0.185			
			0.025	0.338	0.164			
			0.020	0.300	0.146			
			0.015	0.257	0.126			
			0.008	0.156	0.076			

TABLE III (contd.)

A-51.6-2			A-51.6-3			A-51.6-4		
Y(in.)	$\frac{u}{U}$	$\frac{w}{U}$	Y(in.)	$\frac{u}{U}$	$\frac{w}{U}$	Y(in.)	$\frac{u}{U}$	$\frac{w}{U}$
0.386	1.000	0.000	0.561	1.000	0.000	0.634	1.000	0.000
0.361	0.998	0.002	0.541	0.997	0.000	0.584	0.988	0.000
0.336	0.989	0.003	0.521	0.991	0.002	0.534	0.971	0.014
0.311	0.974	0.010	0.501	0.984	0.003	0.484	0.950	0.031
0.291	0.964	0.018	0.481	0.981	0.005	0.434	0.911	0.047
0.271	0.945	0.026	0.461	0.971	0.014	0.384	0.871	0.074
0.251	0.923	0.035	0.441	0.961	0.020	0.334	0.830	0.101
0.231	0.905	0.046	0.421	0.942	0.026	0.314	0.815	0.110
0.211	0.880	0.054	0.401	0.928	0.033	0.294	0.792	0.119
0.191	0.855	0.067	0.381	0.920	0.039	0.274	0.787	0.132
0.171	0.834	0.077	0.361	0.900	0.047	0.254	0.755	0.137
0.151	0.797	0.088	0.341	0.882	0.062	0.234	0.740	0.146
0.141	0.784	0.096	0.321	0.867	0.073	0.214	0.713	0.154
0.131	0.769	0.102	0.301	0.850	0.080	0.194	0.692	0.162
0.121	0.765	0.107	0.281	0.829	0.093	0.174	0.678	0.173
0.111	0.746	0.112	0.261	0.806	0.105	0.154	0.660	0.179
0.101	0.736	0.116	0.241	0.794	0.115	0.134	0.636	0.185
0.091	0.719	0.120	0.221	0.773	0.127	0.124	0.621	0.186
0.081	0.701	0.125	0.201	0.758	0.136	0.114	0.598	0.187
0.071	0.684	0.129	0.181	0.743	0.147	0.104	0.592	0.190
0.061	0.667	0.136	0.161	0.734	0.160	0.094	0.580	0.194
0.051	0.640	0.140	0.151	0.712	0.162	0.084	0.587	0.206
0.041	0.614	0.144	0.141	0.696	0.168	0.074	0.565	0.207
0.033	0.586	0.146	0.131	0.695	0.172	0.064	0.546	0.204
0.023	0.550	0.143	0.121	0.681	0.177	0.054	0.530	0.203
0.018	0.522	0.140	0.111	0.672	0.182	0.046	0.503	0.201
0.013	0.465	0.126	0.101	0.655	0.183	0.036	0.471	0.196
0.008	0.455	0.124	0.091	0.642	0.189	0.026	0.442	0.185
			0.081	0.629	0.193	0.021	0.402	0.168
			0.071	0.611	0.198	0.016	0.342	0.143
			0.061	0.604	0.202	0.011	0.280	0.117
			0.051	0.601	0.210	0.008	0.274	0.115
			0.043	0.573	0.207			
			0.033	0.548	0.203			
			0.028	0.524	0.197			
			0.023	0.504	0.189			
			0.018	0.445	0.167			
			0.013	0.365	0.137			
			0.008	0.354	0.133			

TABLE III (contd.)

A-51.6-5			A-51.6-6			A-51.6-8		
Y(in.)	$\frac{u}{U}$	$\frac{w}{U}$	Y(in.)	$\frac{u}{U}$	$\frac{w}{U}$	Y(in.)	$\frac{u}{U}$	$\frac{w}{U}$
0.799	1.000	0.000	0.943	1.000	0.000	1.321	1.000	0.000
0.749	0.989	0.000	0.893	0.995	0.007	1.271	0.993	0.000
0.699	0.981	0.009	0.843	0.974	0.014	1.221	0.988	0.007
0.649	0.955	0.016	0.793	0.962	0.023	1.171	0.984	0.010
0.599	0.943	0.036	0.743	0.935	0.036	1.121	0.966	0.012
0.549	0.903	0.052	0.693	0.899	0.052	1.071	0.958	0.022
0.499	0.869	0.074	0.643	0.871	0.064	1.021	0.948	0.028
0.449	0.824	0.100	0.593	0.834	0.085	0.971	0.931	0.041
0.424	0.803	0.106	0.543	0.796	0.099	0.946	0.924	0.054
0.399	0.783	0.116	0.493	0.750	0.111	0.921	0.916	0.058
0.374	0.762	0.128	0.443	0.706	0.130	0.896	0.896	0.063
0.349	0.726	0.134	0.393	0.668	0.146	0.871	0.895	0.070
0.329	0.717	0.143	0.368	0.651	0.154	0.821	0.876	0.083
0.309	0.703	0.150	0.343	0.632	0.158	0.771	0.839	0.091
0.289	0.672	0.154	0.318	0.616	0.162	0.721	0.836	0.111
0.269	0.653	0.166	0.293	0.601	0.171	0.671	0.815	0.123
0.249	0.633	0.170	0.268	0.565	0.173	0.621	0.797	0.132
0.229	0.630	0.179	0.243	0.549	0.183	0.571	0.776	0.148
0.209	0.620	0.189	0.218	0.542	0.189	0.521	0.753	0.167
0.189	0.614	0.197	0.193	0.529	0.201	0.471	0.727	0.176
0.169	0.594	0.203	0.173	0.520	0.212	0.421	0.716	0.194
0.149	0.569	0.213	0.153	0.507	0.213	0.371	0.680	0.207
0.139	0.563	0.212	0.133	0.490	0.226	0.321	0.658	0.221
0.129	0.561	0.215	0.113	0.475	0.222	0.271	0.627	0.227
0.119	0.546	0.219	0.093	0.458	0.222	0.221	0.593	0.234
0.109	0.536	0.222	0.083	0.454	0.229	0.171	0.569	0.246
0.099	0.527	0.224	0.073	0.451	0.227	0.146	0.558	0.254
0.089	0.517	0.228	0.063	0.407	0.214	0.121	0.517	0.242
0.079	0.501	0.227	0.053	0.407	0.214	0.096	0.509	0.248
0.069	0.473	0.220	0.043	0.404	0.212	0.071	0.483	0.246
0.059	0.465	0.221	0.035	0.399	0.210	0.046	0.432	0.229
0.051	0.453	0.225	0.025	0.354	0.186	0.023	0.383	0.204
0.041	0.414	0.207	0.015	0.250	0.131	0.013	0.274	0.145
0.036	0.413	0.209	0.008	0.219	0.115	0.008	0.208	0.110
0.031	0.392	0.198						
0.026	0.347	0.176						
0.021	0.294	0.149						
0.016	0.224	0.113						
0.011	0.209	0.106						
0.008	0.200	0.101						

TABLE III (contd.)

B-50.6-1

Y(in.)	$\frac{u}{U}$	$\frac{w}{U}$
0.210	1.000	0.000
0.185	0.974	0.009
0.160	0.941	0.009
0.140	0.904	0.019
0.120	0.866	0.029
0.100	0.827	0.037
0.080	0.779	0.052
0.060	0.728	0.060
0.050	0.682	0.064
0.040	0.647	0.068
0.030	0.595	0.069
0.025	0.563	0.070
0.022	0.504	0.063
0.017	0.353	0.044
0.012	0.198	0.025
0.008	0.144	0.018

B-50.6-2

Y(in.)	$\frac{u}{U}$	$\frac{w}{U}$
0.415	1.000	0.000
0.365	0.997	0.002
0.315	0.969	0.016
0.265	0.920	0.039
0.215	0.859	0.063
0.190	0.814	0.075
0.165	0.787	0.087
0.145	0.756	0.094
0.125	0.726	0.106
0.105	0.670	0.113
0.085	0.653	0.124
0.065	0.641	0.136
0.045	0.604	0.149
0.035	0.568	0.151
0.027	0.521	0.143
0.017	0.484	0.137
0.012	0.443	0.127
0.008	0.319	0.092

B-50.6-3

Y(in.)	$\frac{u}{U}$	$\frac{w}{U}$
0.575	1.000	0.000
0.525	0.986	0.007
0.475	0.982	0.014
0.425	0.950	0.029
0.375	0.908	0.051
0.325	0.857	0.073
0.275	0.814	0.107
0.250	0.751	0.114
0.225	0.744	0.126
0.200	0.710	0.133
0.175	0.694	0.146
0.155	0.673	0.154
0.135	0.641	0.158
0.115	0.630	0.174
0.095	0.602	0.177
0.075	0.561	0.177
0.055	0.543	0.191
0.045	0.508	0.186
0.035	0.484	0.181
0.027	0.424	0.159
0.017	0.274	0.102
0.012	0.207	0.077
0.008	0.156	0.058

B-50.6-4

Y(in.)	$\frac{u}{U}$	$\frac{w}{U}$
0.728	1.000	0.000
0.678	0.989	0.007
0.628	0.970	0.012
0.578	0.966	0.023
0.528	0.925	0.035
0.478	0.906	0.057
0.428	0.861	0.079
0.378	0.825	0.103
0.353	0.807	0.112
0.328	0.752	0.120
0.303	0.740	0.132
0.278	0.728	0.144
0.253	0.714	0.152
0.228	0.656	0.153
0.203	0.654	0.169
0.178	0.628	0.181
0.158	0.619	0.191
0.138	0.589	0.199
0.118	0.565	0.204
0.098	0.553	0.209
0.078	0.525	0.212
0.058	0.463	0.203
0.048	0.450	0.200
0.038	0.458	0.214
0.030	0.380	0.184
0.020	0.335	0.162
0.015	0.291	0.141
0.010	0.251	0.121
0.008	0.213	0.103

TABLE III (contd.)

B-50.6-5			B-50.6-6			B-50.6-7		
Y(in.)	$\frac{u}{U}$	$\frac{w}{U}$	Y(in.)	$\frac{u}{U}$	$\frac{w}{U}$	Y(in.)	$\frac{u}{U}$	$\frac{w}{U}$
0.833	1.000	0.000	1.180	1.000	0.000	1.332	1.000	0.000
0.783	0.991	0.009	1.080	0.984	0.005	1.232	0.986	0.010
0.733	0.985	0.017	0.980	0.982	0.009	1.132	0.961	0.023
0.683	0.963	0.027	0.880	0.950	0.025	1.032	0.930	0.037
0.633	0.926	0.041	0.780	0.911	0.049	0.932	0.898	0.053
0.583	0.904	0.062	0.680	0.855	0.081	0.832	0.856	0.081
0.533	0.867	0.082	0.630	0.822	0.098	0.782	0.838	0.093
0.483	0.822	0.099	0.580	0.783	0.117	0.732	0.821	0.107
0.458	0.800	0.110	0.530	0.747	0.123	0.682	0.789	0.118
0.433	0.779	0.117	0.480	0.717	0.146	0.632	0.756	0.134
0.408	0.765	0.126	0.430	0.673	0.157	0.582	0.737	0.142
0.383	0.748	0.140	0.380	0.664	0.182	0.532	0.705	0.164
0.358	0.720	0.151	0.355	0.648	0.188	0.482	0.681	0.177
0.333	0.700	0.160	0.330	0.628	0.195	0.432	0.662	0.195
0.308	0.693	0.165	0.305	0.607	0.203	0.407	0.643	0.200
0.283	0.672	0.182	0.280	0.589	0.209	0.382	0.633	0.208
0.258	0.639	0.186	0.255	0.565	0.213	0.357	0.618	0.215
0.233	0.609	0.185	0.230	0.545	0.221	0.332	0.602	0.219
0.208	0.589	0.200	0.205	0.539	0.235	0.307	0.594	0.228
0.183	0.573	0.204	0.180	0.508	0.227	0.282	0.562	0.226
0.158	0.539	0.210	0.155	0.475	0.227	0.257	0.550	0.234
0.133	0.525	0.216	0.130	0.497	0.249	0.232	0.540	0.244
0.108	0.504	0.227	0.105	0.459	0.249	0.207	0.530	0.250
0.083	0.489	0.233	0.080	0.448	0.252	0.182	0.536	0.266
0.063	0.456	0.228	0.060	0.415	0.245	0.157	0.506	0.261
0.043	0.410	0.213	0.040	0.368	0.225	0.132	0.483	0.268
0.035	0.404	0.211	0.032	0.360	0.219	0.112	0.450	0.254
0.025	0.345	0.183	0.022	0.321	0.196	0.092	0.451	0.270
0.015	0.223	0.119	0.012	0.231	0.141	0.072	0.425	0.260
0.010	0.216	0.115	0.008	0.181	0.110	0.052	0.408	0.259
0.008	0.191	0.102				0.042	0.381	0.244
						0.034	0.328	0.210
						0.024	0.307	0.197
						0.014	0.225	0.144
						0.008	0.192	0.123

TABLE III (contd.)

B-52.1-1

Y(in.)	$\frac{u}{U}$	$\frac{w}{U}$
0.296	1.000	0.000
0.246	0.994	0.002
0.196	0.974	0.007
0.146	0.901	0.023
0.126	0.861	0.034
0.106	0.832	0.047
0.086	0.799	0.060
0.066	0.754	0.078
0.046	0.692	0.077
0.036	0.624	0.077
0.028	0.597	0.079
0.018	0.519	0.073
0.013	0.453	0.064
0.008	0.226	0.032

B-52.1-2

Y(in.)	$\frac{u}{U}$	$\frac{w}{U}$
0.457	1.000	0.000
0.407	0.990	0.002
0.357	0.964	0.009
0.307	0.926	0.031
0.257	0.864	0.053
0.232	0.840	0.072
0.207	0.798	0.084
0.182	0.766	0.100
0.157	0.757	0.117
0.137	0.715	0.123
0.117	0.700	0.138
0.097	0.668	0.147
0.077	0.637	0.159
0.057	0.605	0.168
0.037	0.565	0.172
0.029	0.505	0.163
0.019	0.472	0.159
0.014	0.421	0.144
0.008	0.418	0.143

B-52.1-3

Y(in.)	$\frac{u}{U}$	$\frac{w}{U}$
0.618	1.000	0.000
0.568	0.988	0.005
0.518	0.972	0.016
0.468	0.933	0.031
0.418	0.894	0.053
0.368	0.837	0.077
0.318	0.802	0.104
0.268	0.743	0.128
0.243	0.713	0.139
0.218	0.699	0.155
0.193	0.678	0.167
0.168	0.647	0.178
0.148	0.612	0.180
0.128	0.597	0.188
0.108	0.562	0.202
0.088	0.530	0.196
0.068	0.539	0.215
0.058	0.504	0.208
0.048	0.487	0.205
0.038	0.478	0.211
0.030	0.437	0.195
0.020	0.382	0.170
0.015	0.245	0.109
0.010	0.187	0.083
0.008	0.153	0.068

B-52.1-4

Y(in.)	$\frac{u}{U}$	$\frac{w}{U}$
0.775	1.000	0.000
0.725	0.984	0.003
0.675	0.970	0.012
0.625	0.945	0.031
0.575	0.920	0.045
0.525	0.873	0.067
0.475	0.841	0.089
0.425	0.788	0.111
0.375	0.763	0.137
0.350	0.730	0.144
0.325	0.709	0.152
0.300	0.672	0.162
0.275	0.666	0.175
0.250	0.634	0.182
0.225	0.638	0.203
0.200	0.605	0.209
0.175	0.573	0.212
0.155	0.535	0.208
0.135	0.536	0.226
0.115	0.495	0.216
0.095	0.496	0.232
0.075	0.487	0.242
0.055	0.439	0.229
0.037	0.412	0.226
0.027	0.385	0.211
0.017	0.312	0.171
0.012	0.254	0.139
0.008	0.213	0.117

TABLE III (contd.)

B-52.1-5			B-52.1-6			B-54.5-1		
Y(in.)	$\frac{u}{U}$	$\frac{w}{U}$	Y(in.)	$\frac{u}{U}$	$\frac{w}{U}$	Y(in.)	$\frac{u}{U}$	$\frac{w}{U}$
1.089	1.000	0.000	1.388	1.000	0.000	0.366	1.000	0.000
0.989	0.993	0.000	1.288	0.989	0.007	0.316	1.000	0.000
0.889	0.961	0.012	1.188	0.974	0.014	0.266	0.999	0.002
0.789	0.933	0.031	1.088	0.982	0.026	0.241	0.994	0.002
0.739	0.905	0.046	0.988	0.946	0.040	0.216	0.990	0.003
0.689	0.871	0.059	0.888	0.883	0.066	0.191	0.966	0.010
0.639	0.844	0.078	0.838	0.865	0.079	0.166	0.936	0.018
0.589	0.810	0.096	0.788	0.849	0.095	0.146	0.904	0.027
0.539	0.764	0.114	0.738	0.809	0.108	0.126	0.869	0.039
0.489	0.732	0.130	0.688	0.773	0.120	0.106	0.830	0.052
0.439	0.679	0.149	0.638	0.769	0.142	0.086	0.790	0.062
0.389	0.630	0.157	0.588	0.730	0.159	0.066	0.744	0.073
0.364	0.626	0.173	0.538	0.706	0.174	0.056	0.728	0.083
0.339	0.608	0.182	0.488	0.675	0.194	0.046	0.686	0.086
0.314	0.602	0.191	0.463	0.659	0.200	0.036	0.653	0.092
0.289	0.591	0.201	0.438	0.647	0.204	0.028	0.607	0.092
0.264	0.562	0.208	0.413	0.635	0.216	0.018	0.532	0.081
0.239	0.537	0.214	0.388	0.605	0.217	0.008	0.282	0.043
0.214	0.537	0.226	0.363	0.596	0.228			
0.189	0.517	0.229	0.338	0.589	0.237			
0.169	0.498	0.233	0.313	0.571	0.241			
0.149	0.469	0.229	0.288	0.554	0.250			
0.129	0.464	0.240	0.263	0.533	0.255			
0.109	0.453	0.244	0.238	0.541	0.273			
0.089	0.439	0.250	0.213	0.523	0.282			
0.069	0.391	0.233	0.188	0.499	0.280			
0.059	0.400	0.246	0.163	0.476	0.281			
0.049	0.352	0.219	0.138	0.459	0.289			
0.039	0.383	0.246	0.113	0.451	0.296			
0.031	0.354	0.227	0.088	0.435	0.307			
0.021	0.296	0.190	0.068	0.408	0.293			
0.016	0.242	0.156	0.058	0.380	0.280			
0.011	0.164	0.105	0.048	0.379	0.288			
0.008	0.122	0.078	0.038	0.366	0.278			
			0.030	0.335	0.254			
			0.020	0.298	0.226			
			0.015	0.262	0.199			
			0.010	0.230	0.174			
			0.008	0.192	0.146			

TABLE III (contd.)

B-54.5-2			B-54.5-3			B-54.5-4		
Y(in.)	$\frac{u}{U}$	$\frac{w}{U}$	Y(in.)	$\frac{u}{U}$	$\frac{w}{U}$	Y(in.)	$\frac{u}{U}$	$\frac{w}{U}$
0.521	1.000	0.000	0.726	1.000	0.000	0.883	1.000	0.000
0.471	0.984	0.000	0.676	0.996	0.002	0.833	0.999	0.003
0.446	0.989	0.002	0.626	0.992	0.007	0.783	0.986	0.009
0.421	0.984	0.003	0.576	0.968	0.012	0.733	0.964	0.018
0.396	0.972	0.009	0.526	0.941	0.033	0.683	0.944	0.033
0.371	0.953	0.018	0.476	0.901	0.051	0.633	0.907	0.049
0.346	0.934	0.031	0.426	0.850	0.076	0.583	0.876	0.068
0.321	0.909	0.045	0.376	0.805	0.101	0.533	0.833	0.093
0.296	0.890	0.062	0.351	0.789	0.114	0.483	0.792	0.113
0.271	0.861	0.079	0.326	0.763	0.125	0.433	0.758	0.138
0.246	0.845	0.080	0.301	0.741	0.140	0.408	0.735	0.149
0.221	0.798	0.112	0.276	0.722	0.155	0.383	0.707	0.156
0.196	0.768	0.131	0.251	0.698	0.169	0.358	0.691	0.170
0.171	0.709	0.131	0.226	0.668	0.183	0.333	0.657	0.176
0.151	0.679	0.146	0.201	0.644	0.192	0.308	0.639	0.188
0.131	0.653	0.153	0.176	0.624	0.208	0.283	0.626	0.183
0.111	0.626	0.164	0.156	0.605	0.214	0.258	0.592	0.205
0.091	0.595	0.173	0.136	0.577	0.217	0.233	0.581	0.216
0.071	0.564	0.187	0.116	0.557	0.227	0.208	0.561	0.224
0.051	0.531	0.195	0.096	0.539	0.238	0.183	0.541	0.230
0.041	0.513	0.198	0.076	0.508	0.236	0.163	0.523	0.237
0.033	0.483	0.197	0.056	0.486	0.242	0.143	0.503	0.241
0.023	0.443	0.189	0.046	0.469	0.242	0.123	0.492	0.250
0.013	0.365	0.160	0.038	0.445	0.239	0.103	0.482	0.261
0.008	0.300	0.131	0.028	0.422	0.228	0.083	0.452	0.253
			0.018	0.351	0.189	0.073	0.443	0.260
			0.013	0.273	0.147	0.063	0.434	0.260
			0.008	0.152	0.082	0.053	0.424	0.261
						0.043	0.405	0.253
						0.035	0.369	0.236
						0.025	0.351	0.225
						0.020	0.321	0.207
						0.015	0.275	0.177
						0.010	0.218	0.140
						0.008	0.186	0.120

TABLE III (contd.)

B-54.5-5			B-54.5-6			B-54.5-7		
Y(in.)	$\frac{u}{U}$	$\frac{w}{U}$	Y(in.)	$\frac{u}{U}$	$\frac{w}{U}$	Y(in.)	$\frac{u}{U}$	$\frac{w}{U}$
1.387	1.000	0.000	1.372	1.000	0.000	1.383	1.000	0.000
1.287	0.994	0.005	1.272	0.988	0.005	1.283	0.998	0.010
1.187	0.985	0.009	1.172	0.971	0.018	1.183	0.982	0.026
1.087	0.972	0.017	1.072	0.930	0.039	1.083	0.947	0.051
0.987	0.945	0.028	0.972	0.881	0.064	0.983	0.908	0.078
0.887	0.904	0.053	0.872	0.876	0.093	0.883	0.873	0.109
0.787	0.856	0.079	0.822	0.820	0.108	0.783	0.824	0.140
0.737	0.819	0.093	0.772	0.789	0.125	0.733	0.811	0.156
0.687	0.792	0.113	0.722	0.761	0.142	0.683	0.777	0.172
0.637	0.755	0.129	0.672	0.738	0.157	0.633	0.756	0.181
0.587	0.726	0.147	0.622	0.714	0.176	0.583	0.735	0.183
0.537	0.695	0.167	0.572	0.692	0.192	0.533	0.713	0.211
0.487	0.669	0.185	0.522	0.674	0.213	0.483	0.665	0.218
0.437	0.639	0.202	0.472	0.649	0.231	0.433	0.665	0.242
0.412	0.614	0.212	0.447	0.642	0.244	0.383	0.632	0.253
0.387	0.593	0.210	0.422	0.630	0.251	0.333	0.601	0.265
0.362	0.581	0.226	0.397	0.619	0.263	0.283	0.581	0.281
0.337	0.574	0.235	0.372	0.603	0.267	0.258	0.562	0.275
0.312	0.551	0.240	0.347	0.600	0.267	0.233	0.557	0.286
0.287	0.531	0.248	0.322	0.585	0.286	0.208	0.544	0.292
0.262	0.521	0.254	0.297	0.568	0.291	0.183	0.519	0.293
0.237	0.506	0.263	0.272	0.557	0.299	0.158	0.511	0.300
0.212	0.488	0.270	0.247	0.549	0.312	0.133	0.493	0.300
0.187	0.488	0.271	0.222	0.538	0.321	0.108	0.470	0.305
0.167	0.467	0.282	0.197	0.512	0.218	0.083	0.454	0.307
0.147	0.455	0.290	0.172	0.498	0.323	0.063	0.420	0.292
0.127	0.441	0.293	0.147	0.480	0.326	0.043	0.383	0.279
0.107	0.424	0.293	0.122	0.464	0.327	0.033	0.369	0.276
0.087	0.407	0.297	0.097	0.446	0.334	0.025	0.345	0.258
0.067	0.392	0.299	0.072	0.418	0.326	0.015	0.304	0.228
0.057	0.385	0.295	0.052	0.401	0.324	0.010	0.251	0.187
0.047	0.368	0.292	0.034	0.353	0.285	0.008	0.238	0.178
0.039	0.353	0.289	0.024	0.300	0.242			
0.029	0.310	0.254	0.019	0.279	0.225			
0.019	0.265	0.216	0.014	0.237	0.192			
0.009	0.211	0.172	0.008	0.195	0.158			
0.008	0.163	0.133						

TABLE III (contd.)

B-59.0-1			B-59.0-2			B-59.0-3		
Y(in.)	$\frac{u}{U}$	$\frac{w}{U}$	Y(in.)	$\frac{u}{U}$	$\frac{w}{U}$	Y(in.)	$\frac{u}{U}$	$\frac{w}{U}$
0.391	1.000	0.000	0.956	1.000	0.000	0.957	1.000	0.000
0.341	0.986	0.005	0.856	0.998	0.002	0.857	0.981	0.010
0.291	0.958	0.020	0.756	0.991	0.004	0.757	0.947	0.033
0.241	0.904	0.051	0.706	0.985	0.009	0.657	0.898	0.065
0.216	0.871	0.072	0.656	0.974	0.012	0.607	0.868	0.086
0.191	0.844	0.090	0.606	0.958	0.018	0.557	0.829	0.110
0.166	0.794	0.111	0.556	0.932	0.039	0.507	0.796	0.133
0.141	0.753	0.128	0.506	0.896	0.059	0.457	0.758	0.159
0.116	0.711	0.144	0.456	0.848	0.086	0.407	0.725	0.186
0.091	0.669	0.160	0.406	0.812	0.120	0.357	0.678	0.208
0.066	0.629	0.178	0.356	0.766	0.149	0.332	0.666	0.220
0.041	0.579	0.188	0.306	0.720	0.180	0.307	0.641	0.232
0.031	0.570	0.185	0.281	0.697	0.193	0.282	0.629	0.245
0.023	0.537	0.175	0.256	0.672	0.208	0.257	0.614	0.255
0.018	0.516	0.168	0.231	0.650	0.224	0.232	0.598	0.269
0.013	0.493	0.160	0.206	0.627	0.238	0.207	0.588	0.282
0.008	0.463	0.150	0.181	0.599	0.249	0.182	0.565	0.291
			0.156	0.583	0.260	0.157	0.551	0.301
			0.131	0.559	0.274	0.132	0.534	0.315
			0.106	0.537	0.285	0.107	0.505	0.316
			0.081	0.507	0.288	0.082	0.486	0.322
			0.056	0.477	0.292	0.057	0.465	0.329
			0.036	0.442	0.285	0.037	0.435	0.320
			0.026	0.414	0.274	0.027	0.396	0.293
			0.018	0.369	0.245	0.019	0.355	0.263
			0.013	0.338	0.224	0.009	0.183	0.136
			0.008	0.288	0.190	0.008	0.157	0.116

TABLE III (contd.)

B-59.0-4

Y(in.)	$\frac{u}{U}$	$\frac{w}{U}$
1.363	1.000	0.000
1.263	0.990	0.010
1.163	0.980	0.017
1.063	0.967	0.027
0.963	0.944	0.036
0.863	0.918	0.063
0.763	0.884	0.088
0.663	0.838	0.119
0.613	0.812	0.130
0.563	0.781	0.150
0.513	0.750	0.161
0.463	0.718	0.179
0.413	0.696	0.193
0.363	0.661	0.203
0.313	0.633	0.221
0.288	0.609	0.223
0.263	0.595	0.232
0.238	0.581	0.238
0.213	0.565	0.245
0.188	0.544	0.249
0.163	0.529	0.258
0.138	0.506	0.266
0.113	0.477	0.266
0.088	0.466	0.275
0.063	0.437	0.275
0.043	0.401	0.261
0.033	0.388	0.261
0.025	0.344	0.233
0.020	0.315	0.214
0.015	0.282	0.191
0.010	0.209	0.142
0.008	0.174	0.118

B-59.6-1

Y(in.)	$\frac{u}{U}$	$\frac{w}{U}$
0.426	1.000	0.000
0.376	0.991	0.005
0.326	0.966	0.018
0.276	0.919	0.041
0.251	0.880	0.060
0.226	0.841	0.072
0.201	0.811	0.086
0.176	0.767	0.102
0.151	0.711	0.112
0.126	0.669	0.120
0.101	0.619	0.119
0.076	0.596	0.159
0.051	0.562	0.165
0.028	0.512	0.159
0.018	0.460	0.143
0.008	0.372	0.115

B-59.6-2

Y(in.)	$\frac{u}{U}$	$\frac{w}{U}$
0.738	1.000	0.000
0.688	0.998	0.007
0.638	0.974	0.016
0.588	0.933	0.031
0.538	0.912	0.051
0.488	0.861	0.079
0.438	0.821	0.113
0.388	0.770	0.144
0.338	0.726	0.179
0.313	0.705	0.189
0.288	0.679	0.207
0.263	0.653	0.218
0.238	0.629	0.230
0.213	0.612	0.246
0.188	0.592	0.260
0.163	0.567	0.269
0.138	0.536	0.278
0.113	0.515	0.286
0.088	0.495	0.298
0.063	0.463	0.298
0.038	0.428	0.291
0.030	0.419	0.288
0.020	0.382	0.267
0.010	0.316	0.220
0.008	0.299	0.209

TABLE III (contd.)

B-59.6-3			B-59.6-4			B-59.6-5		
Y(in.)	$\frac{u}{U}$	$\frac{w}{U}$	Y(in.)	$\frac{u}{U}$	$\frac{w}{U}$	Y(in.)	$\frac{u}{U}$	$\frac{w}{U}$
1.050	1.000	0.000	1.358	1.000	0.000	1.371	1.000	0.000
0.950	0.998	0.000	1.258	0.988	0.003	1.271	0.978	0.019
0.850	0.979	0.012	1.158	0.972	0.012	1.171	0.964	0.030
0.800	0.963	0.025	1.058	0.953	0.029	1.071	0.942	0.051
0.750	0.942	0.041	0.958	0.914	0.060	0.971	0.921	0.074
0.700	0.916	0.061	0.858	0.868	0.092	0.871	0.884	0.102
0.650	0.880	0.083	0.758	0.818	0.125	0.771	0.844	0.133
0.600	0.850	0.104	0.658	0.772	0.167	0.721	0.830	0.153
0.550	0.811	0.128	0.608	0.744	0.187	0.671	0.804	0.169
0.500	0.771	0.152	0.558	0.730	0.212	0.621	0.794	0.189
0.450	0.742	0.183	0.508	0.708	0.232	0.571	0.763	0.206
0.425	0.724	0.198	0.458	0.677	0.249	0.521	0.741	0.221
0.400	0.704	0.213	0.408	0.660	0.275	0.471	0.724	0.235
0.375	0.687	0.227	0.358	0.641	0.296	0.421	0.699	0.250
0.350	0.670	0.237	0.308	0.624	0.318	0.371	0.681	0.271
0.325	0.650	0.249	0.258	0.603	0.337	0.346	0.672	0.280
0.300	0.640	0.256	0.233	0.591	0.347	0.321	0.658	0.287
0.275	0.624	0.270	0.208	0.574	0.354	0.296	0.647	0.296
0.250	0.607	0.283	0.183	0.565	0.364	0.271	0.631	0.298
0.225	0.591	0.294	0.158	0.543	0.369	0.246	0.624	0.310
0.200	0.578	0.306	0.133	0.539	0.381	0.221	0.604	0.313
0.175	0.559	0.316	0.108	0.516	0.385	0.196	0.592	0.321
0.150	0.551	0.328	0.083	0.490	0.387	0.171	0.574	0.326
0.125	0.526	0.329	0.058	0.470	0.388	0.146	0.547	0.345
0.100	0.513	0.342	0.048	0.443	0.377	0.121	0.543	0.342
0.075	0.493	0.346	0.038	0.429	0.376	0.096	0.525	0.342
0.050	0.462	0.347	0.030	0.401	0.354	0.071	0.500	0.345
0.040	0.450	0.342	0.020	0.347	0.305	0.061	0.485	0.346
0.032	0.429	0.329	0.010	0.200	0.176	0.051	0.470	0.343
0.022	0.385	0.296	0.008	0.197	0.174	0.041	0.448	0.333
0.017	0.358	0.275				0.033	0.432	0.321
0.012	0.296	0.227				0.023	0.358	0.268
0.008	0.278	0.214				0.013	0.272	0.203
						0.008	0.211	0.158

TABLE III (contd.)

B-59.6-6

Y(in.)	$\frac{u}{U}$	$\frac{w}{U}$
1.377	1.000	0.000
1.277	0.980	0.036
1.177	0.959	0.057
1.077	0.933	0.082
0.977	0.904	0.107
0.877	0.873	0.135
0.777	0.838	0.161
0.677	0.800	0.189
0.577	0.762	0.215
0.527	0.739	0.233
0.477	0.719	0.242
0.427	0.693	0.256
0.377	0.672	0.269
0.327	0.644	0.284
0.277	0.618	0.299
0.252	0.599	0.303
0.227	0.574	0.302
0.202	0.552	0.302
0.177	0.562	0.322
0.152	0.536	0.322
0.127	0.530	0.328
0.102	0.507	0.328
0.077	0.477	0.327
0.057	0.452	0.321
0.037	0.414	0.308
0.029	0.379	0.281
0.019	0.309	0.229
0.009	0.215	0.160
0.008	0.186	0.138

TABLE IV

Tabulation of Momentum Intergal Quantities

Run & Port	δ_x in.	θ_x in.	H_x	δ_z in.	θ_z in.	θ_{xz} in.	θ_{zx} in.
A-45.2-1	0.026	0.018	1.444	0.008	0.001	0.003	0.004
2	0.048	0.034	1.412	0.015	0.002	0.004	0.011
3	0.095	0.058	1.638	0.028	0.003	0.008	0.020
4	0.111	0.074	1.500	0.043	0.005	0.012	0.031
5	0.157	0.100	1.570	0.059	0.008	0.020	0.038
6	0.178	0.105	1.695	0.072	0.010	0.024	0.047
7	0.204	0.126	1.619	0.080	0.011	0.027	0.053
8	0.263	0.164	1.604	0.118	0.021	0.042	0.076
9	0.265	0.164	1.616	0.120	0.020	0.041	0.079
A-51.6-1	0.030	0.022	1.364	0.009	0.001	0.002	0.006
2	0.065	0.047	1.383	0.026	0.003	0.008	0.019
3	0.101	0.078	1.295	0.052	0.008	0.015	0.037
4	0.134	0.091	1.472	0.064	0.009	0.021	0.043
5	0.194	0.118	1.641	0.087	0.015	0.031	0.056
6	0.260	0.152	1.709	0.110	0.018	0.043	0.067
B-50.6-1	0.047	0.025	1.880	0.007	0.001	0.001	0.006
2	0.071	0.057	1.246	0.029	0.004	0.008	0.021
3	0.123	0.077	1.597	0.052	0.008	0.013	0.038
4	0.159	0.107	1.486	0.076	0.013	0.030	0.045
5	0.205	0.130	1.577	0.100	0.018	0.037	0.063
6	0.279	0.168	1.661	0.136	0.026	0.051	0.084
7	0.324	0.203	1.596	0.172	0.030	0.063	0.109
B-52.1-1	0.044	0.028	1.571	0.010	0.001	0.003	0.007
2	0.088	0.060	1.467	0.035	0.005	0.011	0.025
3	0.147	0.089	1.652	0.065	0.010	0.023	0.043
4	0.199	0.117	1.701	0.095	0.017	0.035	0.060
5	0.278	0.162	1.716	0.123	0.023	0.048	0.075
6	0.333	0.198	1.682	0.186	0.039	0.074	0.112

TABLE IV (contd.)

Run & Port	δ_x in.	Θ_x in.	H_x	δ_z in.	Θ_z in.	Θ_{xz} in.	Θ_{zx} in.
B-54.5-1	0.050	0.024	2.083	0.010	0.001	0.003	0.008
2	0.105	0.060	1.750	0.045	0.007	0.017	0.028
3	0.162	0.099	1.636	0.080	0.016	0.028	0.052
4	0.228	0.134	1.701	0.124	0.024	0.054	0.070
5	0.341	0.194	1.758	0.176	0.037	0.072	0.104
6	0.323	0.198	1.631	0.222	0.050	0.079	0.143
7	0.374	0.212	1.764	0.218	0.053	0.086	0.132
B-59.0-1	0.074	0.050	1.480	0.035	0.008	0.008	0.027
2	0.176	0.114	1.544	0.106	0.025	0.039	0.067
3	0.231	0.145	1.593	0.147	0.035	0.055	0.091
4	0.314	0.179	1.754	0.165	0.032	0.058	0.107
B-59.6-1	0.087	0.056	1.554	0.034	0.005	0.011	0.023
2	0.191	0.114	1.675	0.113	0.026	0.044	0.069
3	0.234	0.147	1.592	0.161	0.042	0.056	0.105
4	0.310	0.198	1.566	0.233	0.066	0.084	0.149
5	0.291	0.193	1.508	0.229	0.058	0.076	0.154
6	0.306	0.205	1.493	0.250	0.058	0.078	0.172

TABLE V

Polar Plot Parameters and Other Variables for Each Boundary Layer Traverse

Run & Port	A	ϵ	U ft/sec	β_w (deg)	ψ (deg)	γ_w (deg)	C_f	Ps-Pa in.H_2O
A-45.2-1			40.8	52.2	45.2	7.0		-0.250
2			36.3	56.0	44.9	11.1		-0.179
3			32.7	58.6	44.4	14.2		-0.134
4			30.9	61.7	43.5	18.2		-0.107
5			29.1	63.0	42.4	20.6		-0.083
6			27.8	62.0	40.8	21.2		-0.065
7			26.0	61.0	39.6	21.4		-0.050
8			25.3	65.1	38.2	26.9		-0.037
9			24.7	64.9	39.0	25.9		-0.029
A-51.6-1	0.294	0.182	45.2	60.0	51.6	8.4		-0.302
2	0.441	0.270	41.1	66.7	51.5	15.2	0.0043	-0.244
3	0.567	0.378	38.5	69.5	50.2	19.3	0.0040	-0.188
4	0.607	0.415	34.5	72.0	49.3	22.7	0.0035	-0.128
5	0.532	0.490	32.9	75.0	48.1	26.9	0.0030	-0.102
6			31.0	70.0	45.2	24.8		-0.083
8				68.0	40.0	28.0		-0.050
10				70.0	40.2	29.8		-0.023
B-50.6-1	0.216	0.125	43.9	57.7	50.6	7.1	0.0042	-0.282
2	0.383	0.287	40.5	65.6	49.6	16.0	0.0040	-0.220
3	0.475	0.374	37.2	68.6	48.1	20.5	0.0034	-0.168
4	0.512	0.483	34.8	72.8	47.0	25.8	0.0032	-0.131
5	0.538	0.534	32.6	73.7	45.6	28.1	0.0029	-0.101
6	0.516	0.610	31.5	74.0	42.6	31.4	0.0026	-0.082
7	0.564	0.640	30.8	73.2	40.6	32.6	0.0027	-0.062
B-52.1-1	0.303	0.140	48.2	60.1	52.1	8.0	0.0042	-0.344
2	0.444	0.342	43.5	71.0	52.1	18.9	0.0039	-0.248
3	0.511	0.445	40.3	74.2	50.2	24.0	0.0030	-0.191
4	0.528	0.548	38.1	77.5	48.8	28.7	0.0028	-0.153
5	0.474	0.642	36.1	78.9	46.2	32.7	0.0025	-0.122
6	0.592	0.759	35.4	79.8	42.6	37.2	0.0027	-0.103

TABLE V (contd.)

Run & Port	A	ϵ	U ft/sec	β_w (deg)	ψ (deg)	γ_w (deg)	C_f	Ps-Pa in.H_2O
B-54.5-1	0.300	0.151	53.2	63.1	54.5	8.6	0.0045	-0.420
2	0.436	0.437	48.2	78.1	54.5	23.6	0.0033	-0.298
3	0.542	0.538	43.9	79.7	51.4	28.3	0.0030	-0.228
4	0.526	0.644	42.0	82.4	49.6	32.8	0.0027	-0.191
5	0.544	0.818	40.6	84.8	45.5	39.3	0.0025	-0.151
6	0.673	0.806	38.4	82.9	44.0	38.9	0.0029	-0.122
7	0.740	0.748	37.2	80.8	44.0	36.8	0.0028	-0.091
B-59.0-1	0.523	0.325	62.9	77.0	59.0	18.0	0.0037	-0.578
2	0.635	0.662	58.5	89.5	56.0	33.5	0.0029	-0.434
3	0.673	0.740	54.4	90.0	53.5	36.5	0.0030	-0.347
4	0.698	0.677	50.3	87.0	52.9	34.1	0.0026	-0.251
B-59.0-1	0.432	0.309	67.3	76.8	59.6	17.2	0.0030	-0.644
2	0.630	0.698	62.0	91.0	56.1	34.9	0.0028	-0.507
3	0.714	0.767	58.7	91.5	54.0	37.5	0.0031	-0.443
4	0.793	0.882	52.9	92.2	50.8	41.4	0.0035	-0.320
5	0.857	0.748	49.7	87.2	50.4	36.8	0.0033	-0.225
6	1.050	0.742	46.8	84.8	48.2	36.6	0.0031	-0.176
B-62.4-1			66.9	84.9	62.4			-0.622
2				96.0				-0.495
3				96.0				-0.397
4				94.9				-0.298
5				91.0				-0.215
6				89.0				-0.170
7				88.5				-0.125
8				85.9				-0.090
9				84.2				-0.057
10				82.1				-0.033

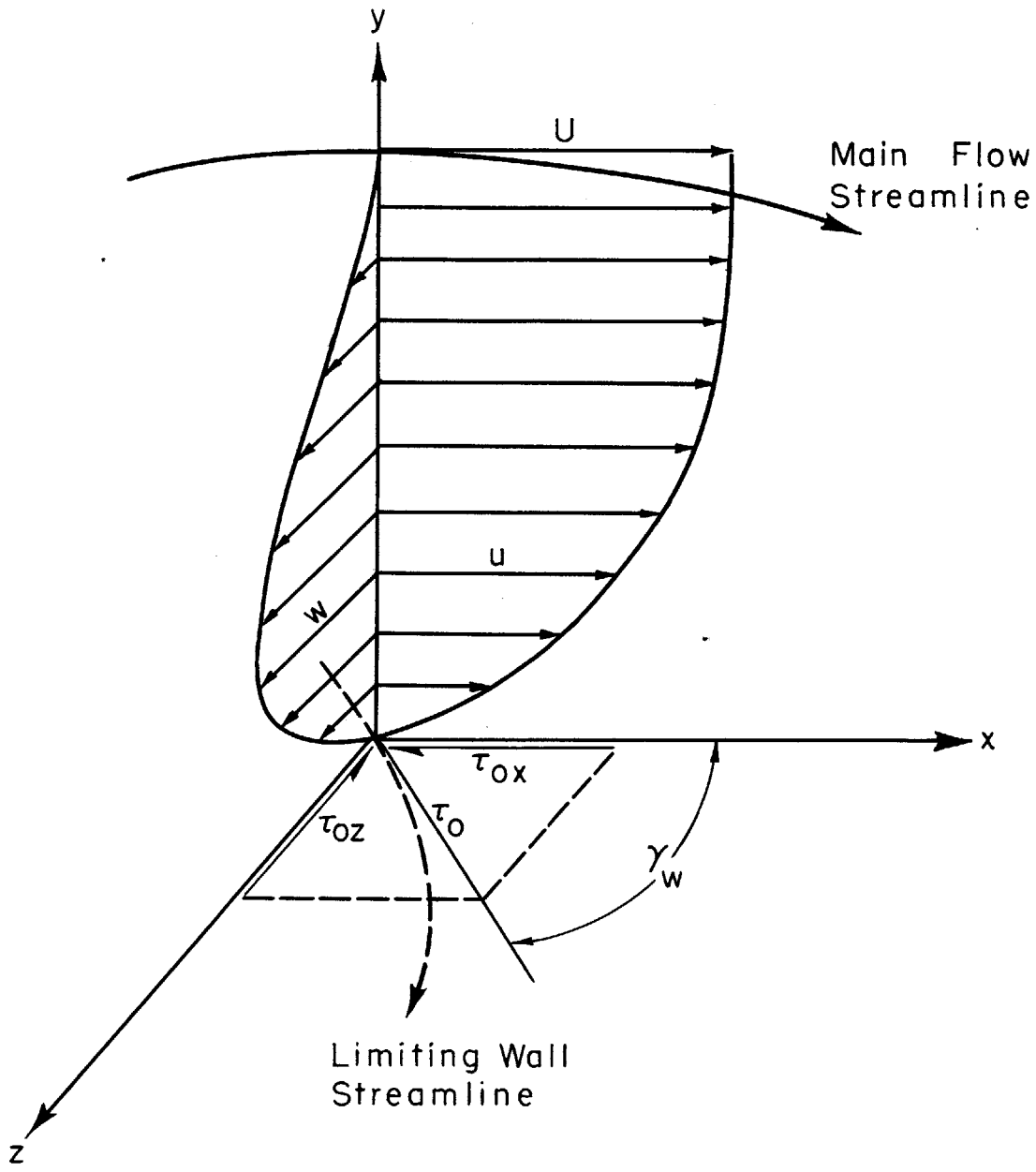

FIGURE 1 - TYPICAL THREE DIMENSIONAL BOUNDARY LAYER

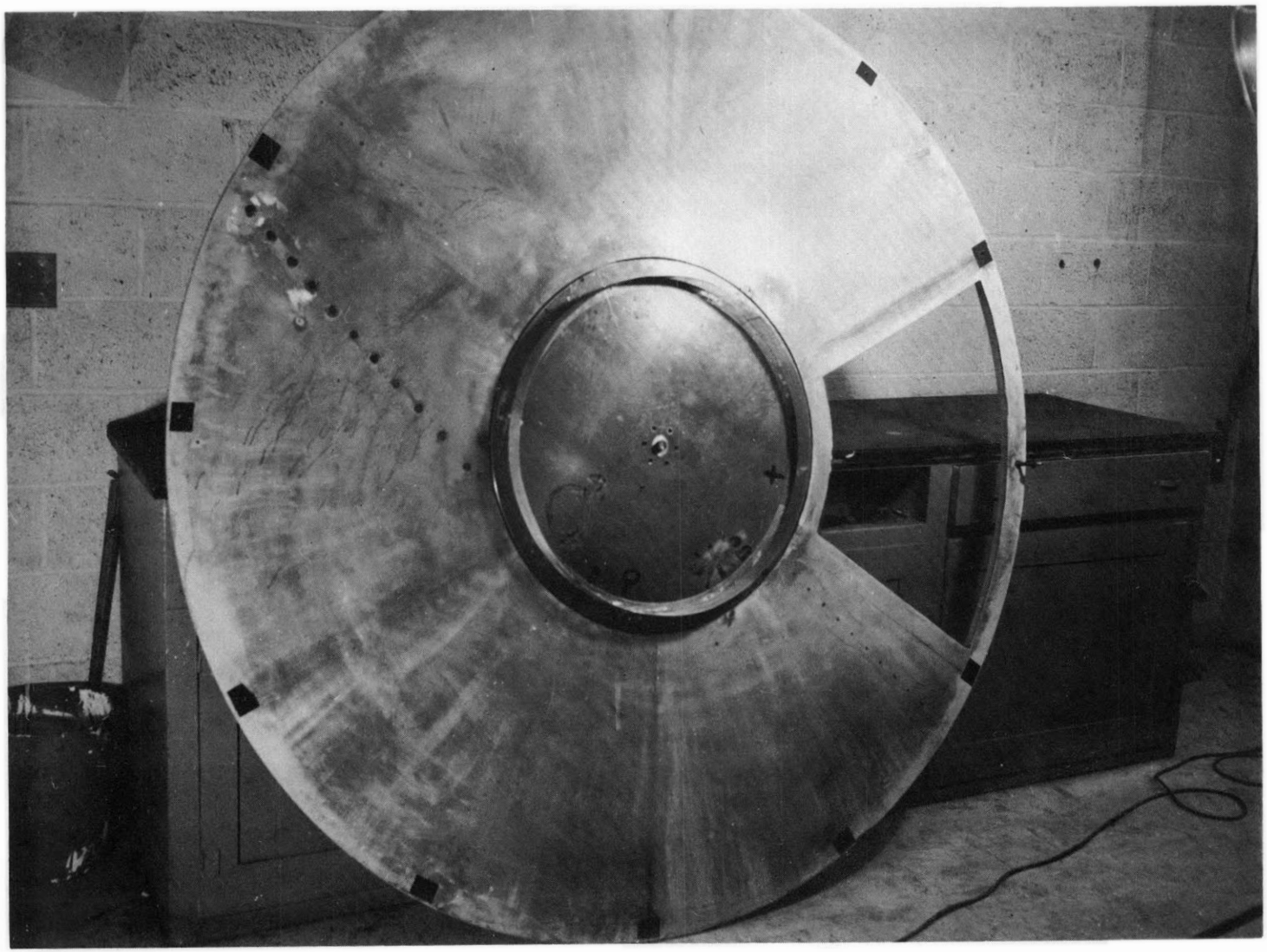

FIGURE 2

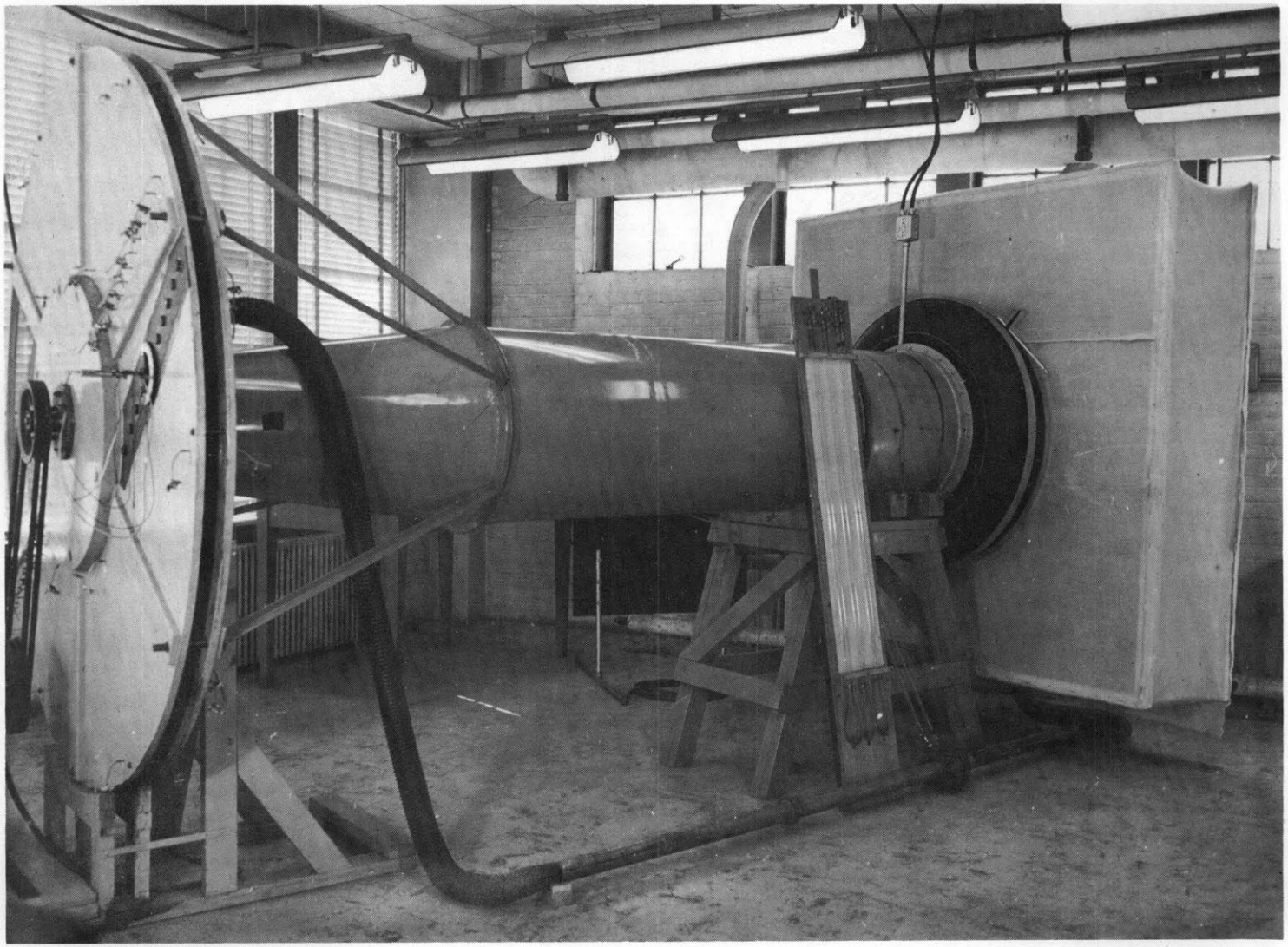

FIGURE 3

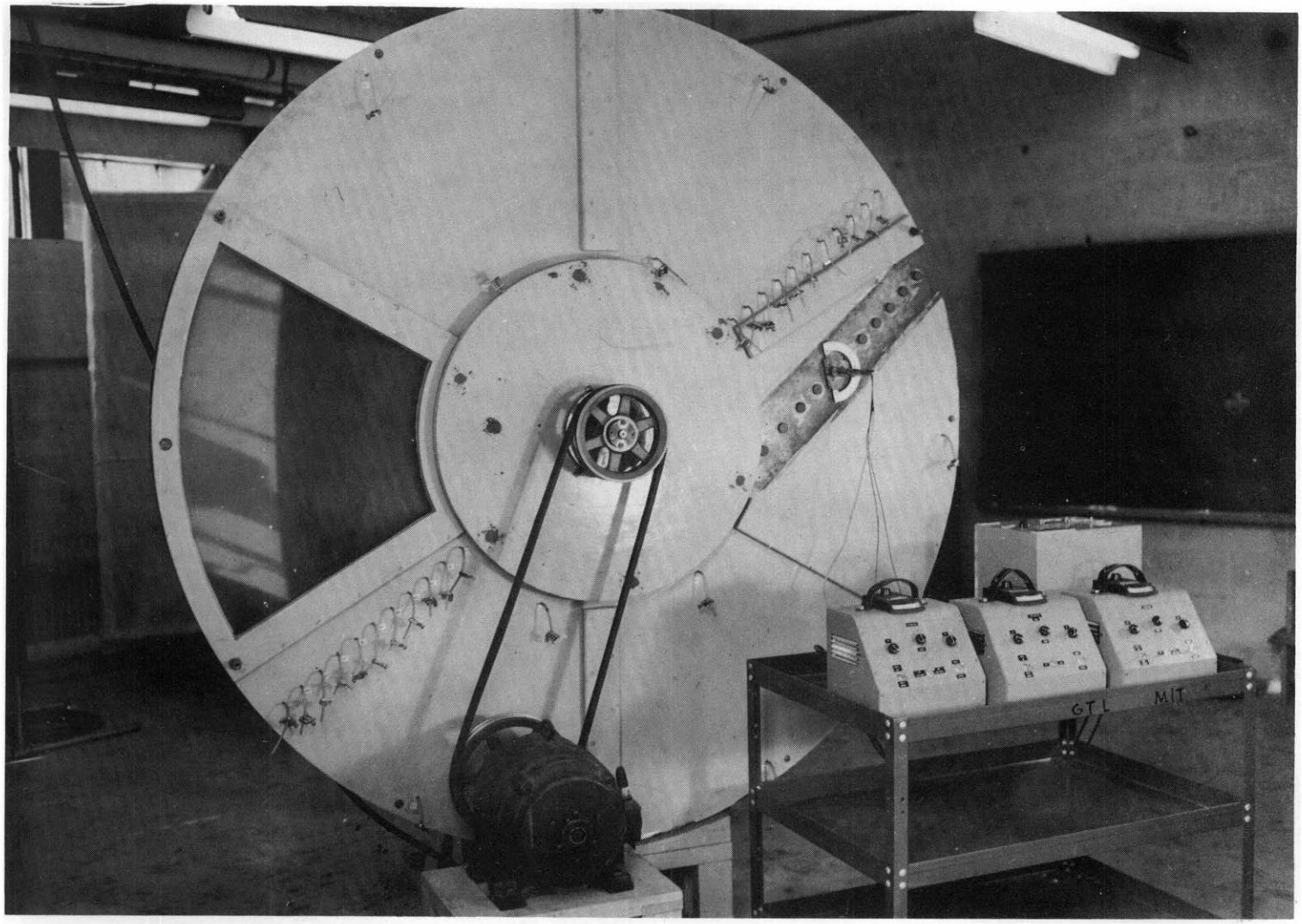

FIGURE 4

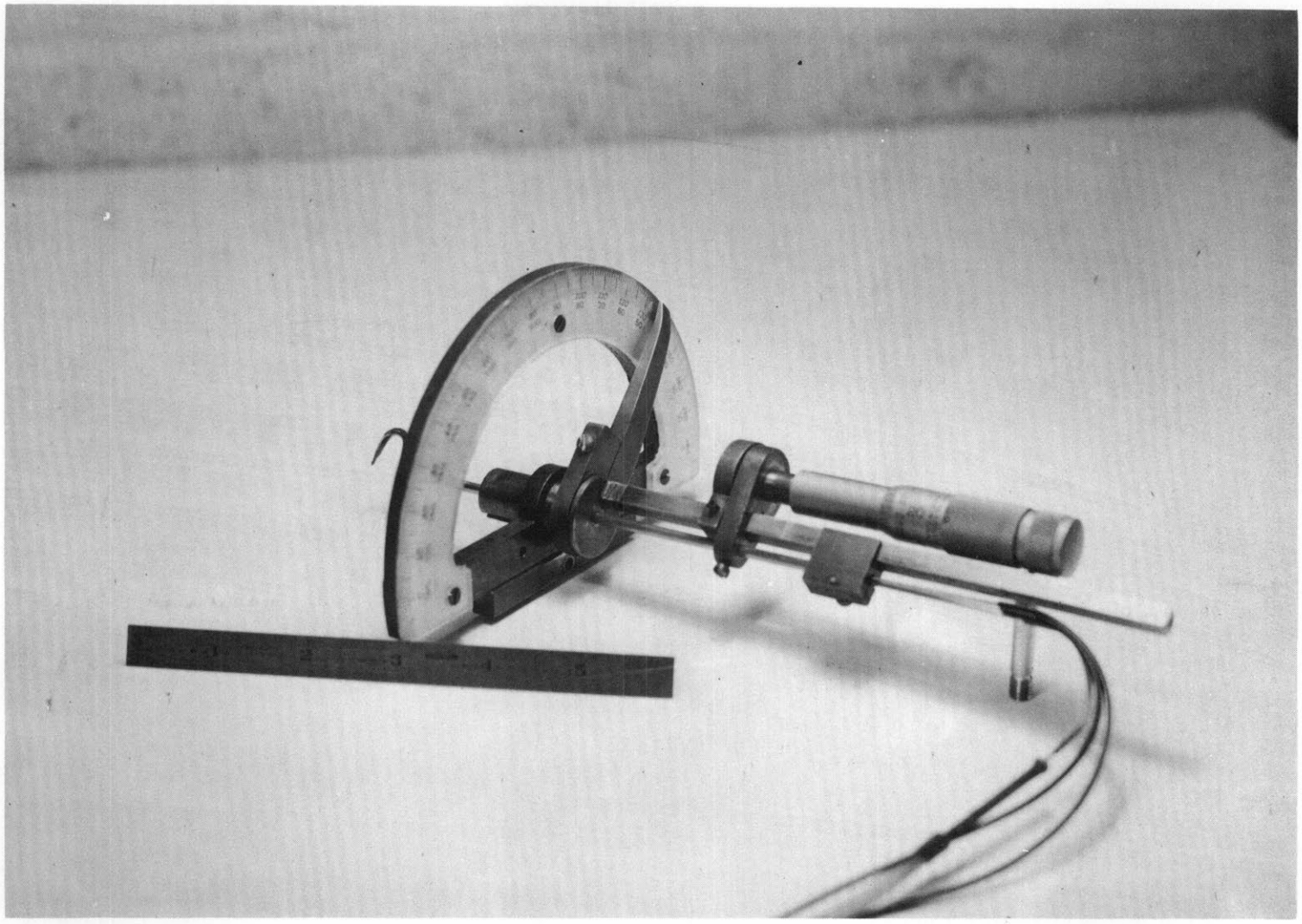

FIGURE 5

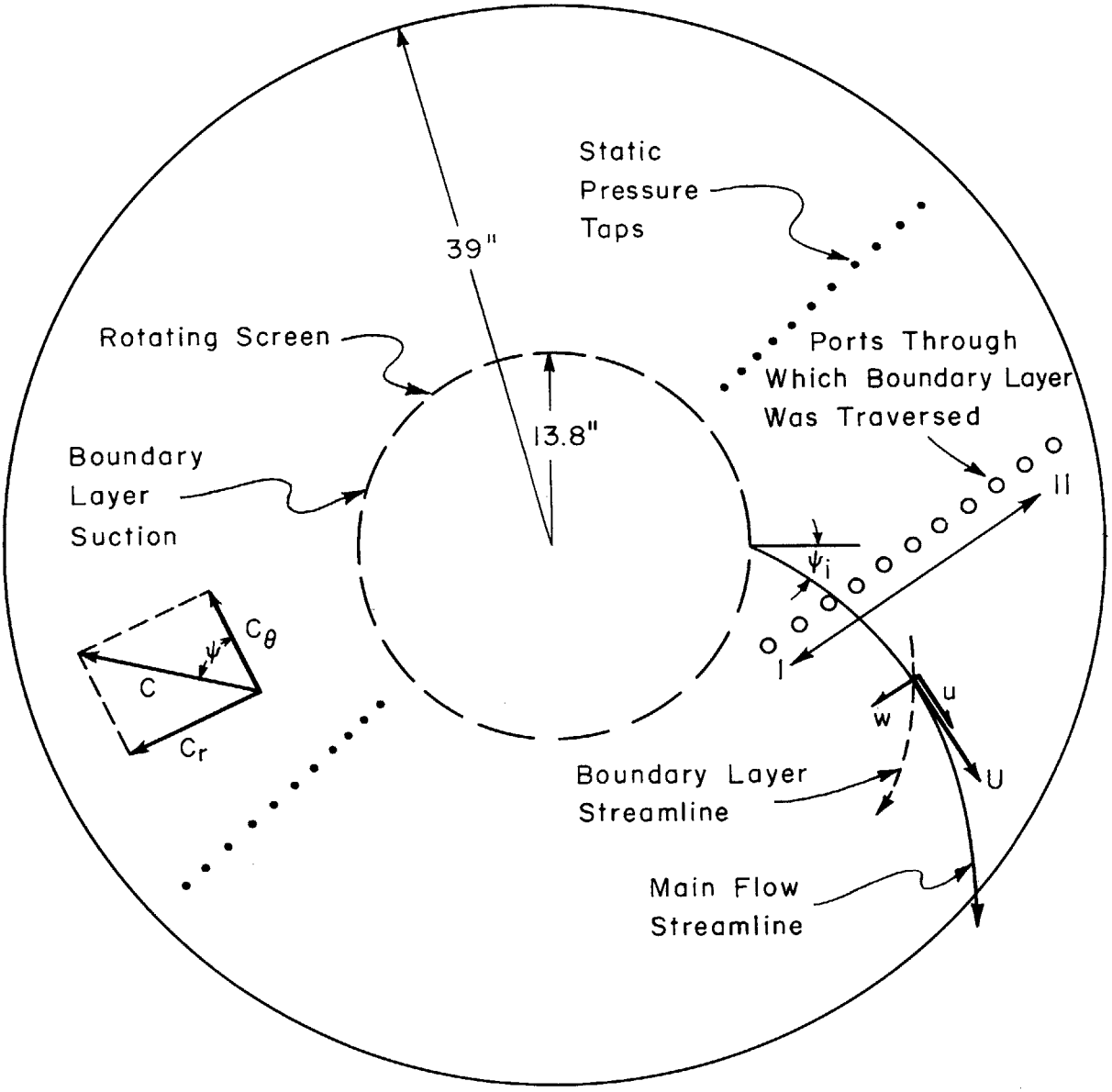

FIGURE 6 – DIAGRAM OF TEST SECTION WITH VELOCITY VECTOR NOTATION

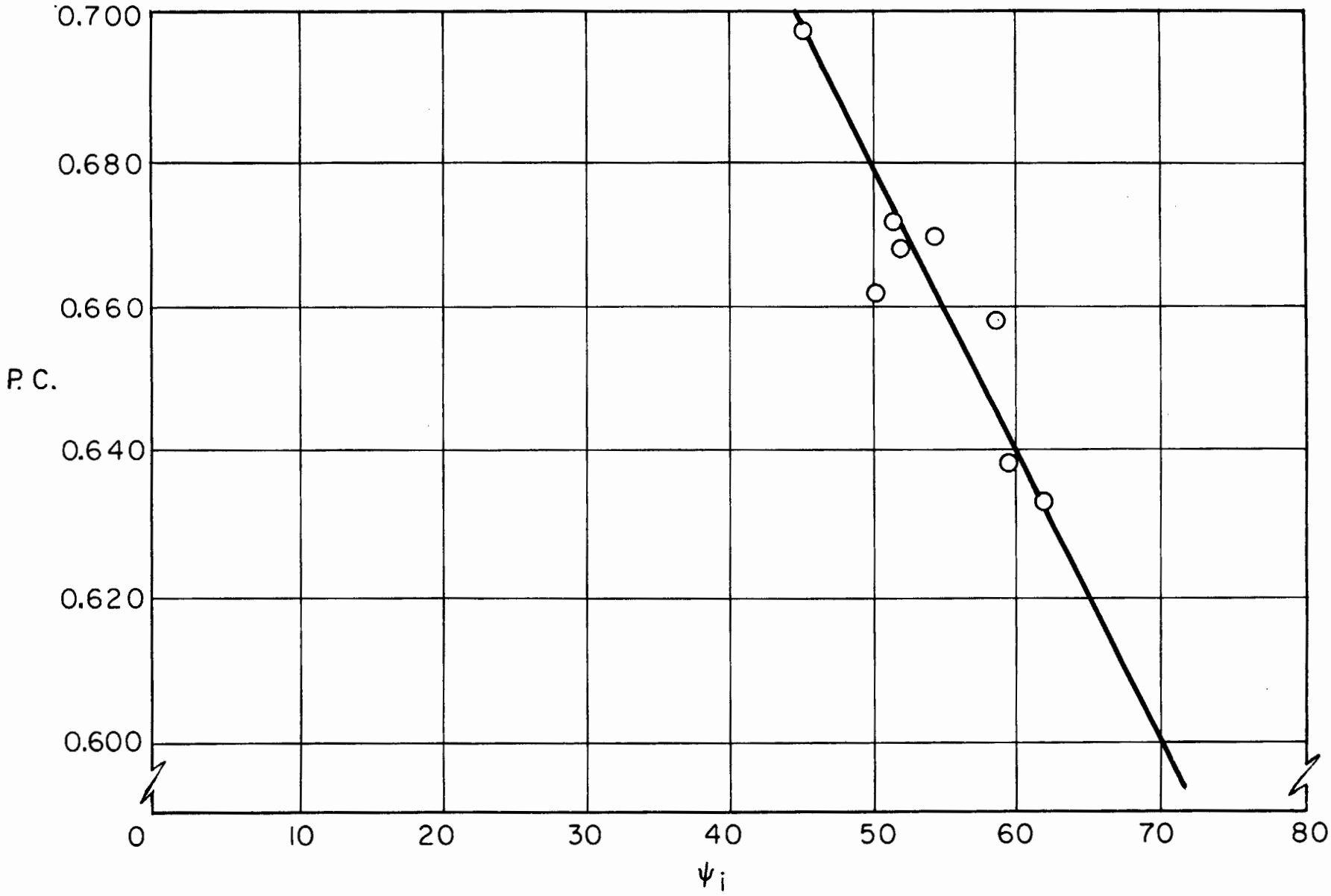

FIGURE 7 - DIFFUSER PRESSURE COEFFICIENT VS INITIAL INLET SWIRL ANGLE

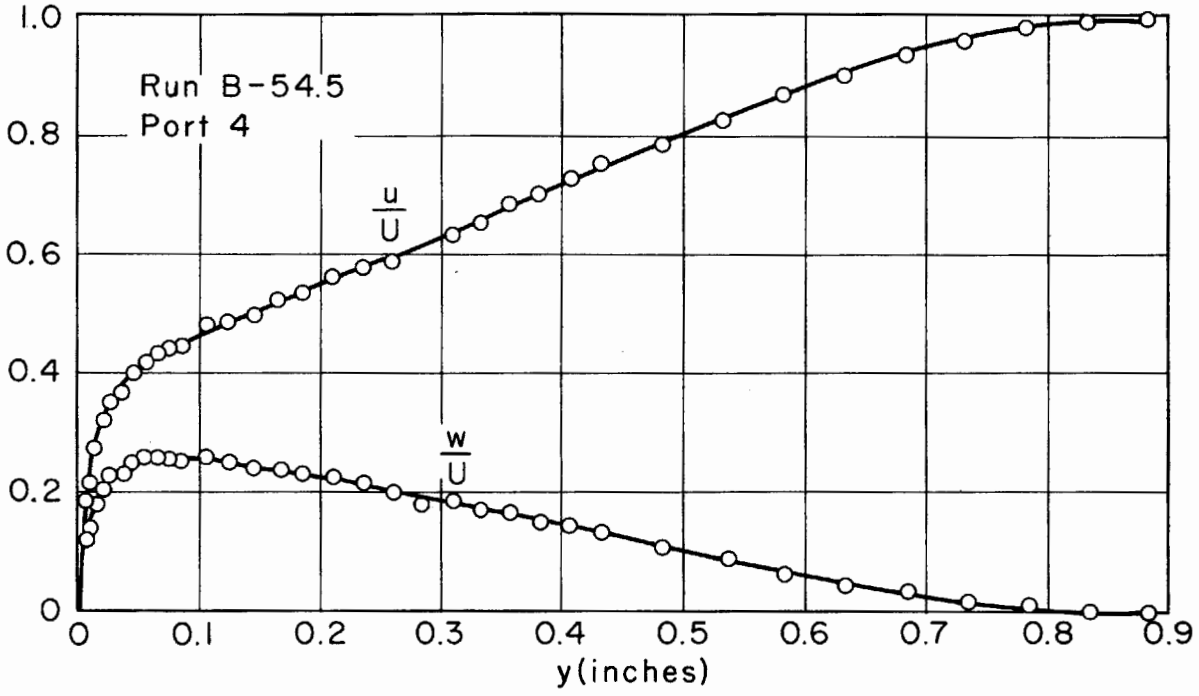

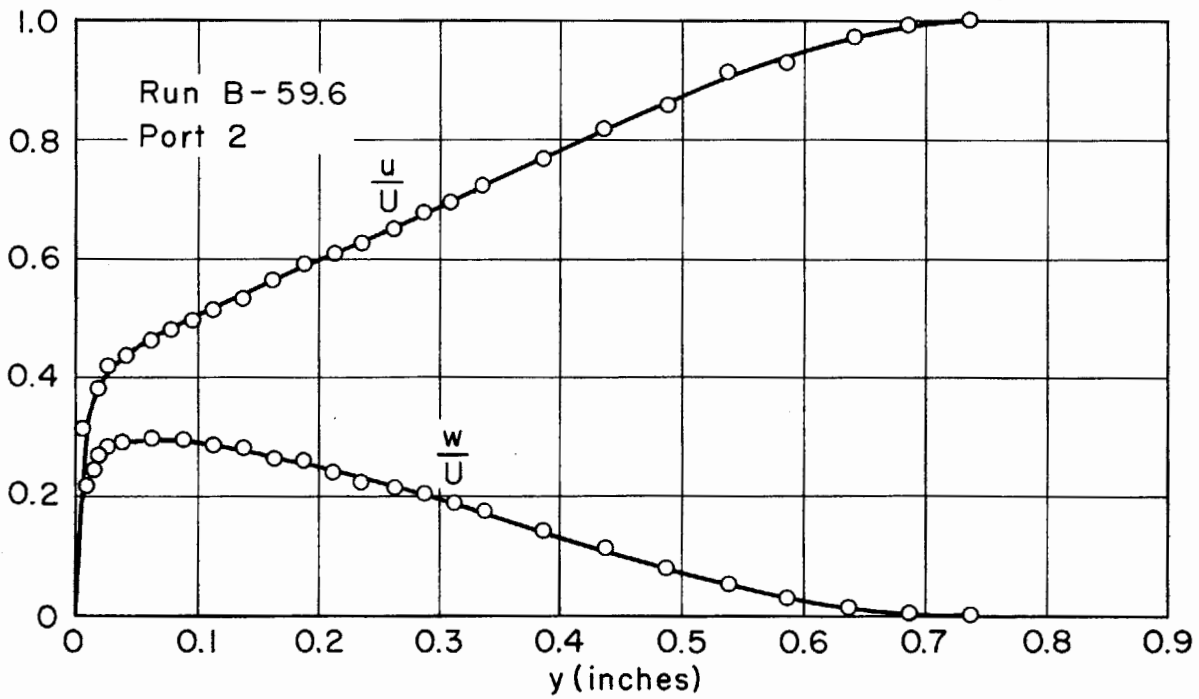

FIGURE 8-SAMPLE VELOCITY PROFILES

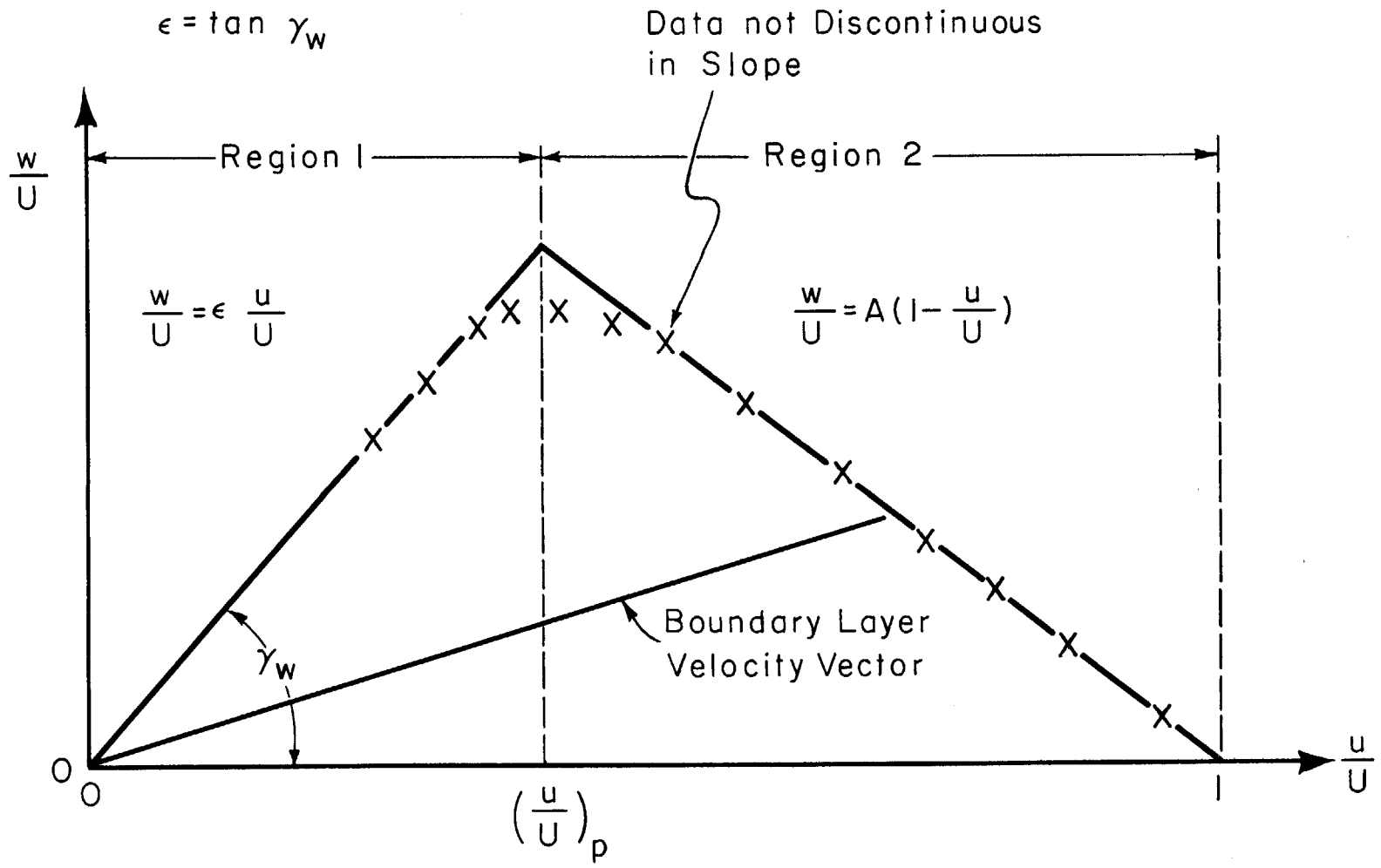

FIGURE 9- DIAGRAM OF VELOCITY POLAR PLOT

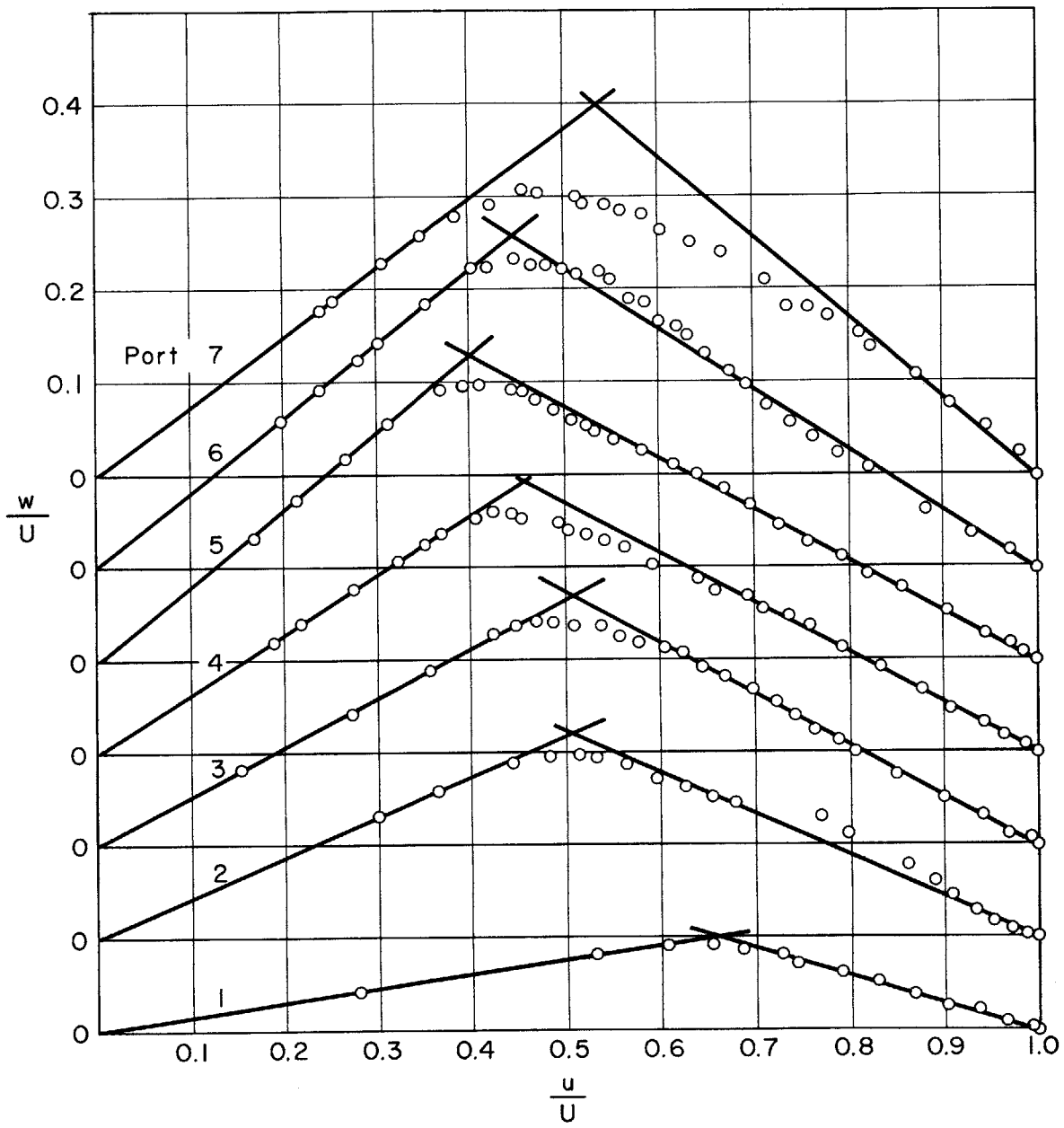

FIGURE 10a - VELOCITY POLAR PLOTS - RUN B-54.5

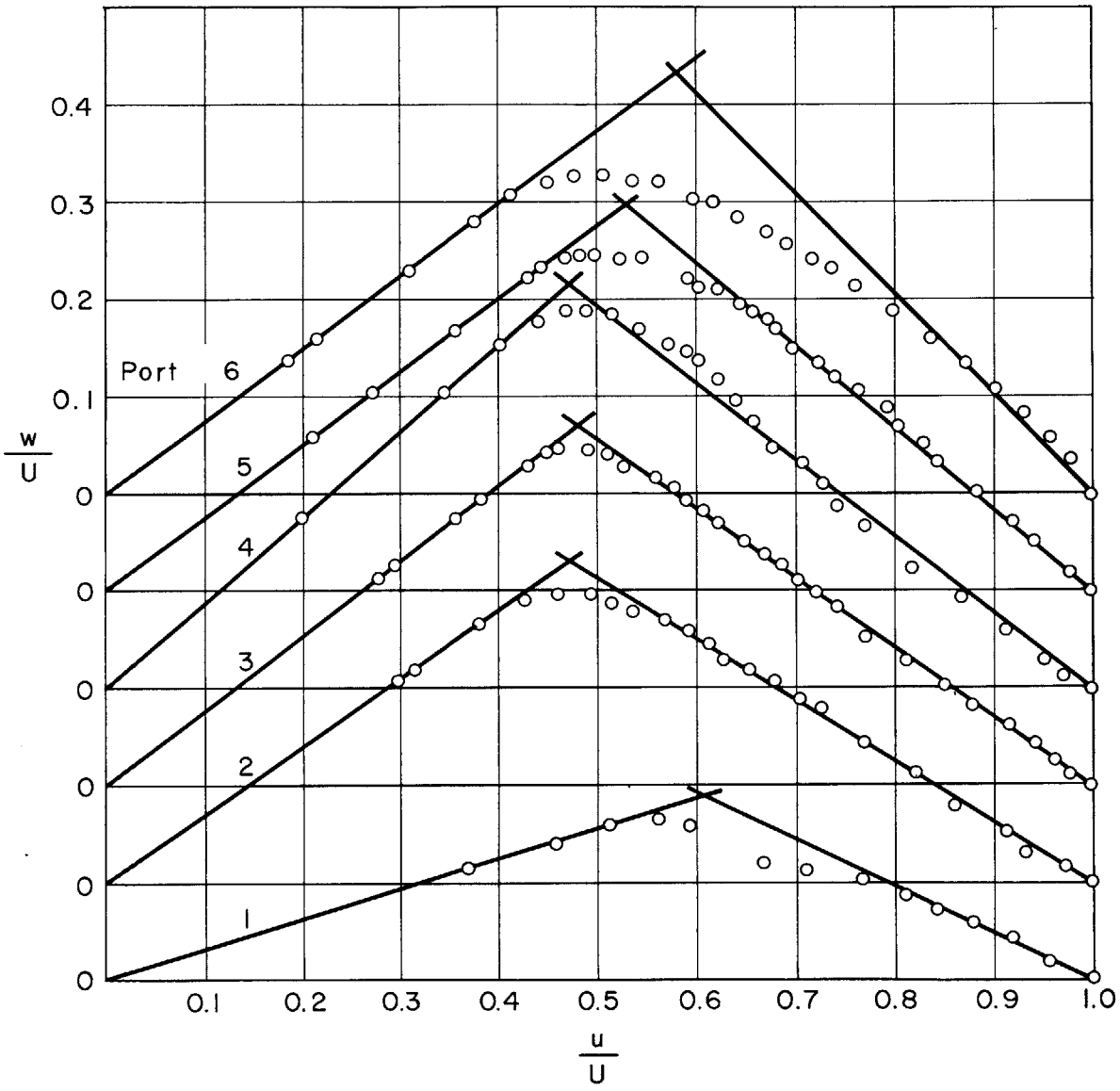

FIGURE 10b – VELOCITY POLAR PLOTS – RUN B-59.6

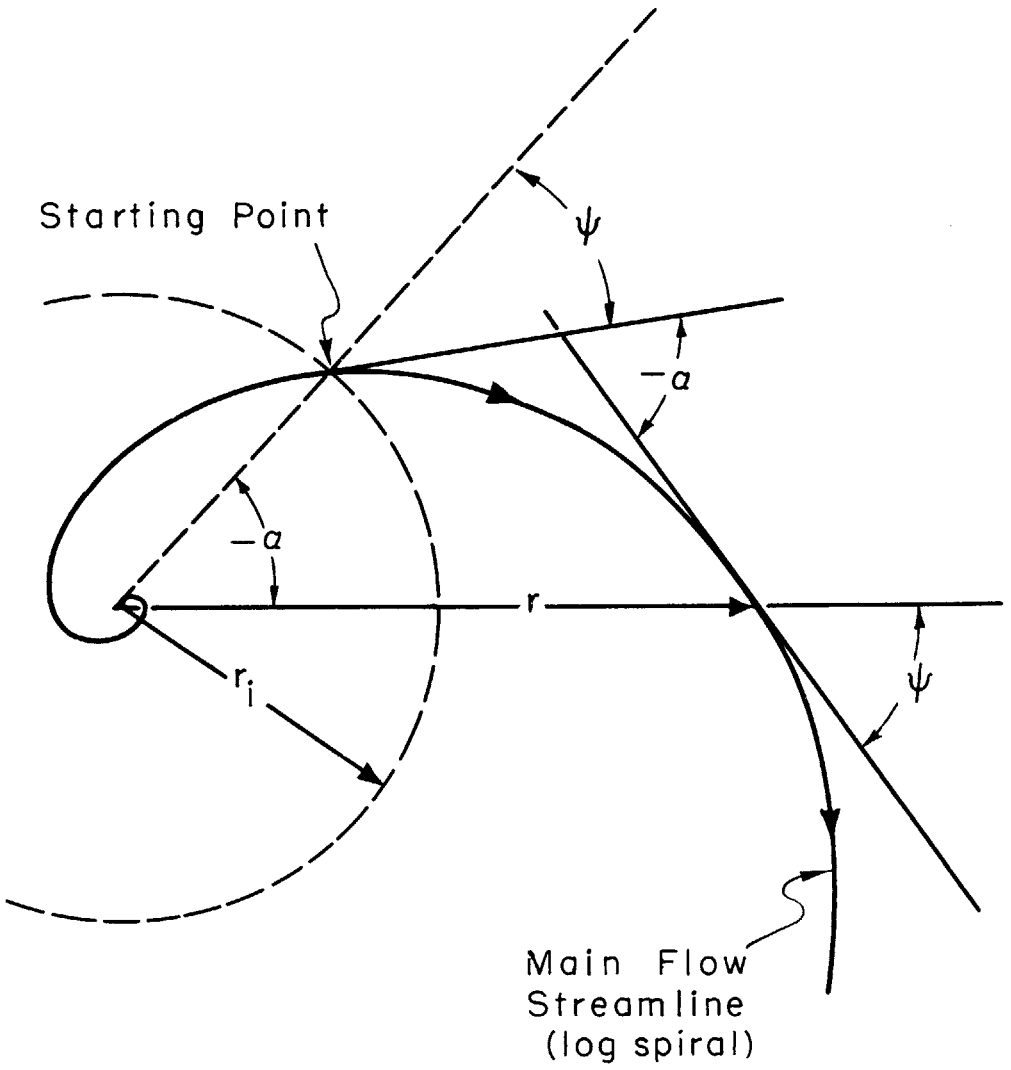

FIGURE II- NOMENCLATURE FOR DERIVATION OF THE PARAMETER A.

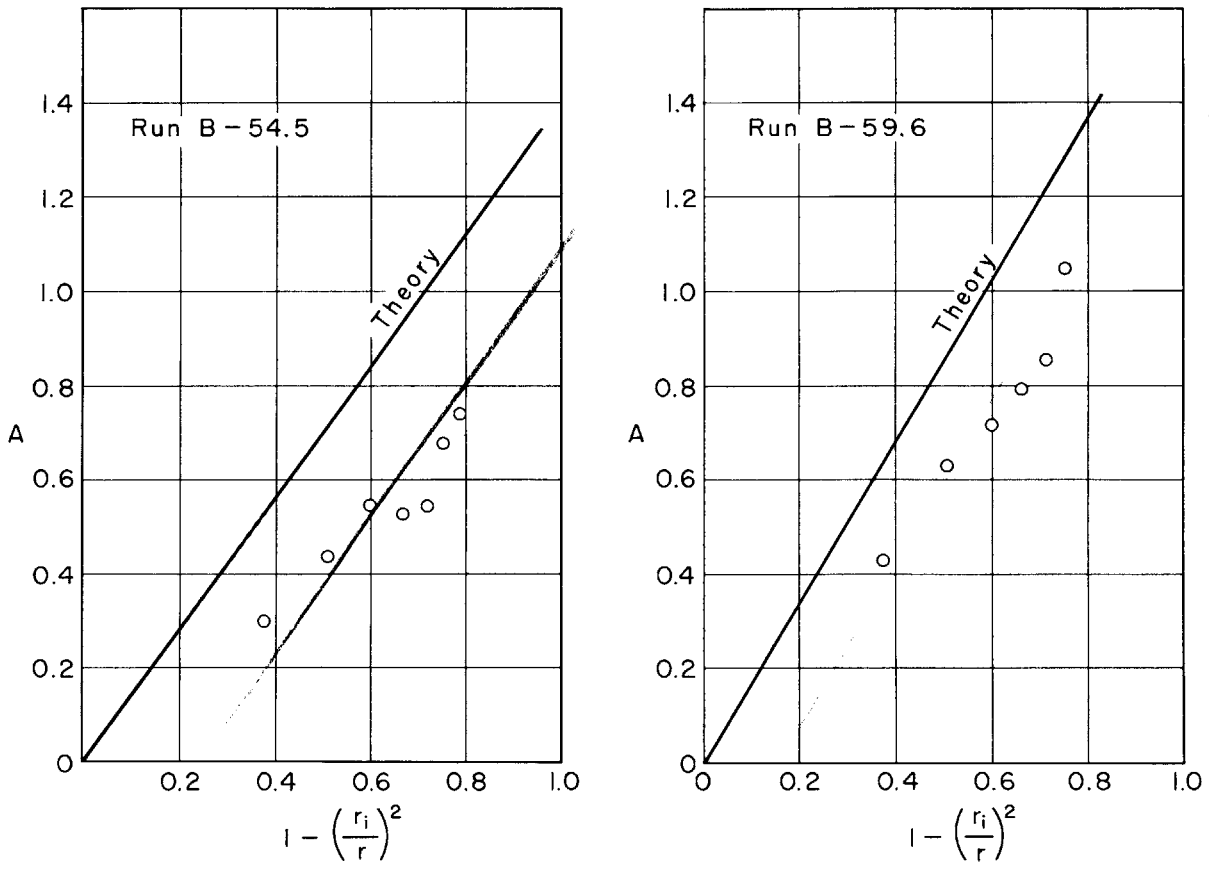

FIGURE 12-CORRELATION OF THE PARAMETER A

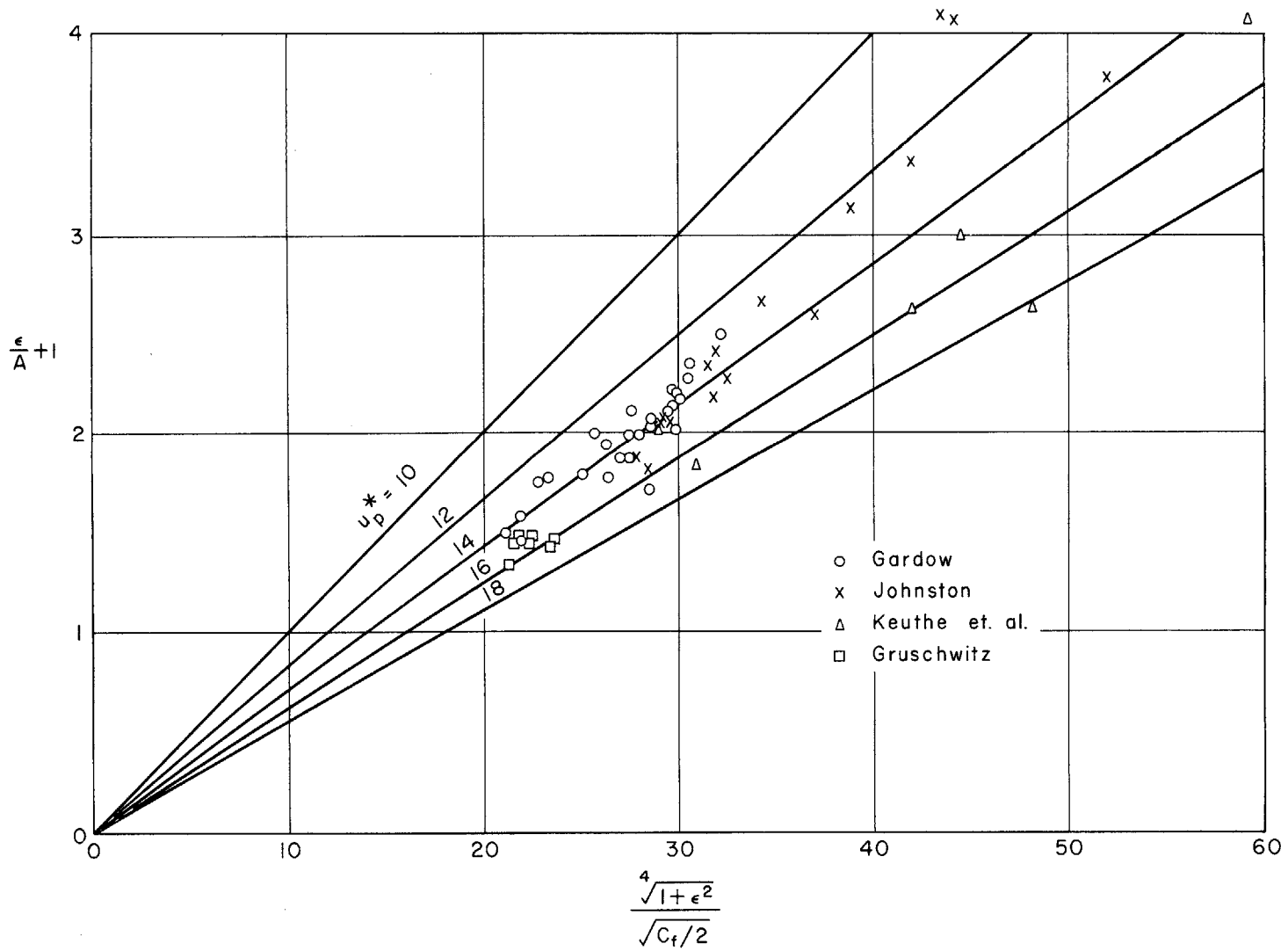

FIGURE 13 – $\frac{\epsilon}{A}+1$ VS $\frac{\sqrt[4]{1+\epsilon^2}}{\sqrt{C_f/2}}$ WITH $\frac{u_p}{\sqrt{\tau_{ox}/\rho}}$ AS PARAMETER

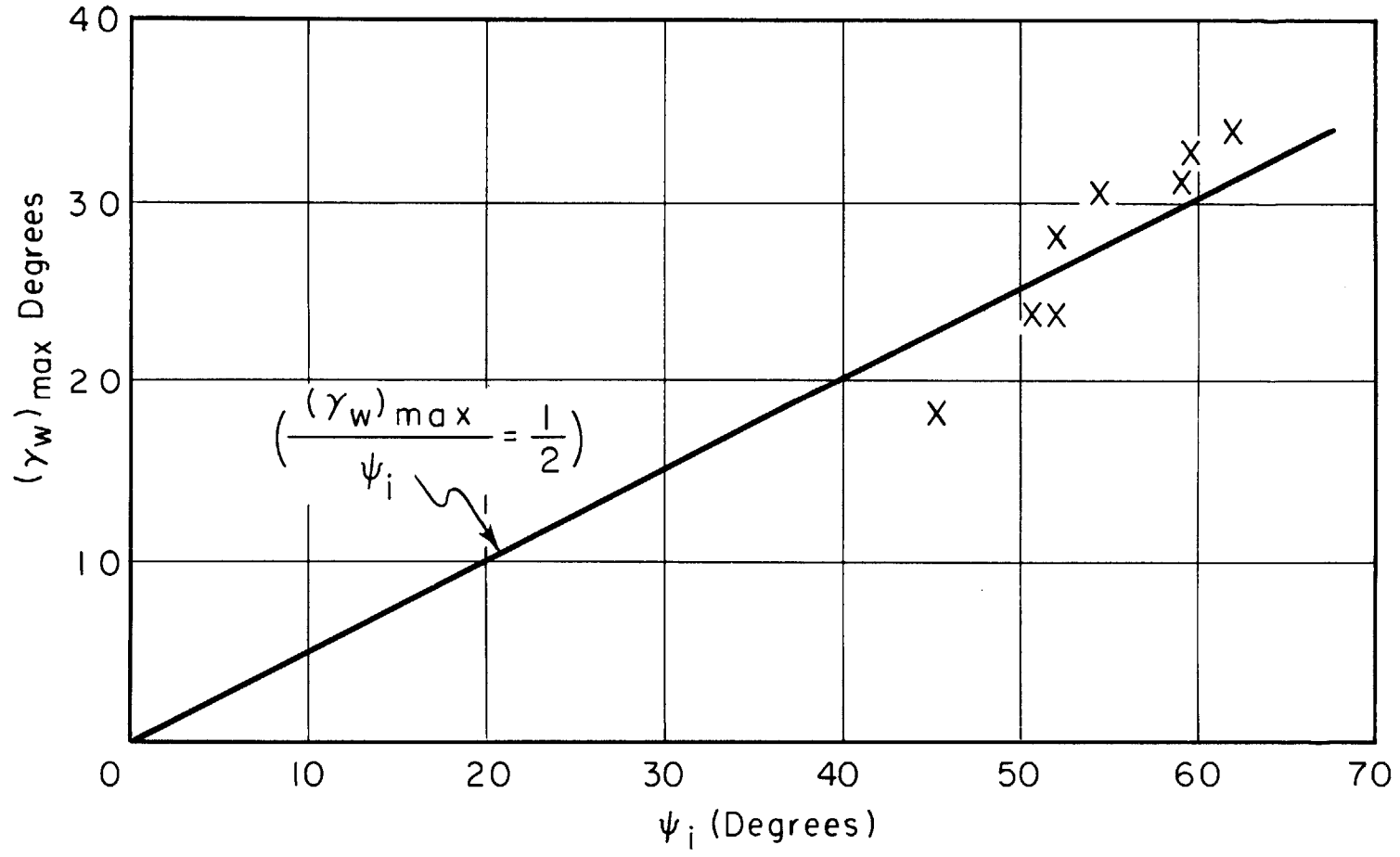

FIGURE 14 - $(\gamma_w)_{max}$ VS. ψ_i

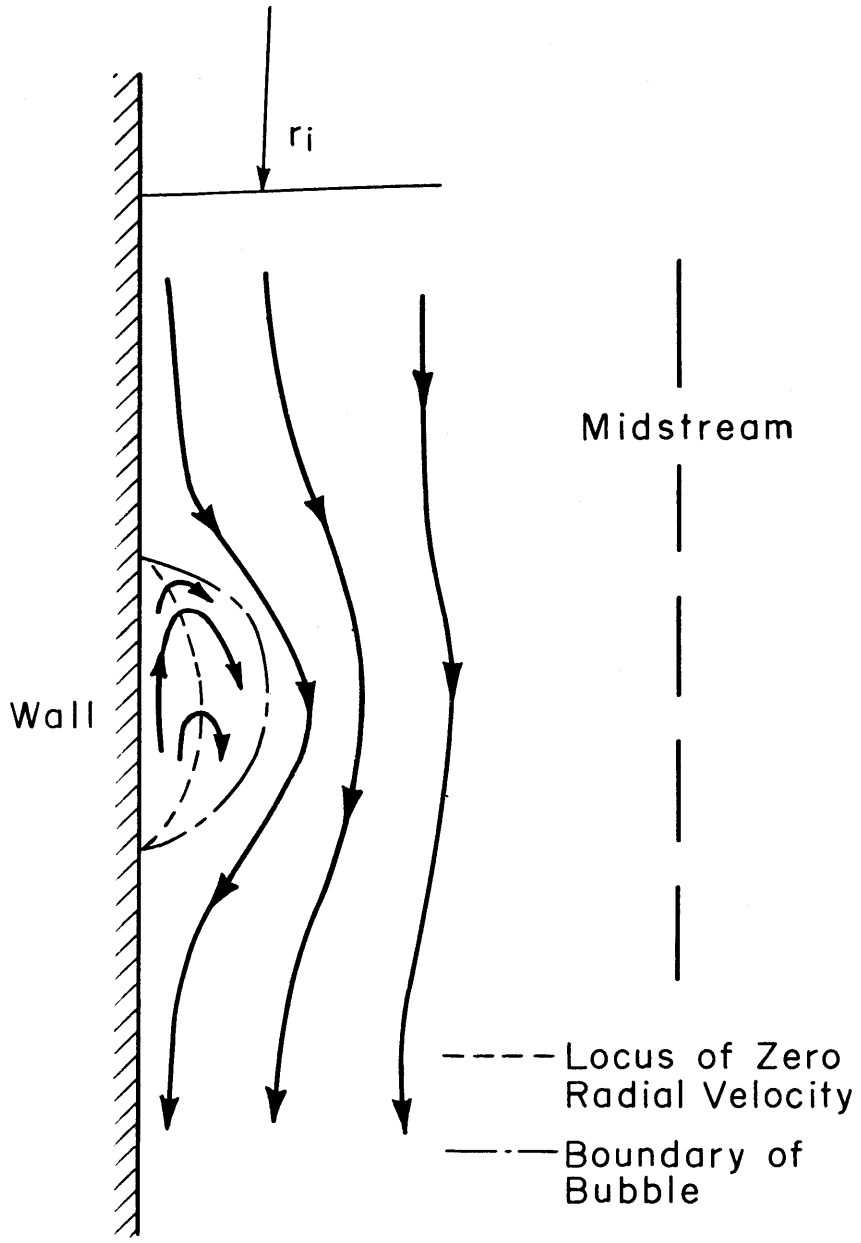

FIGURE 15–RADIAL COMPONENT OF VELOCITY IN DIFFUSER

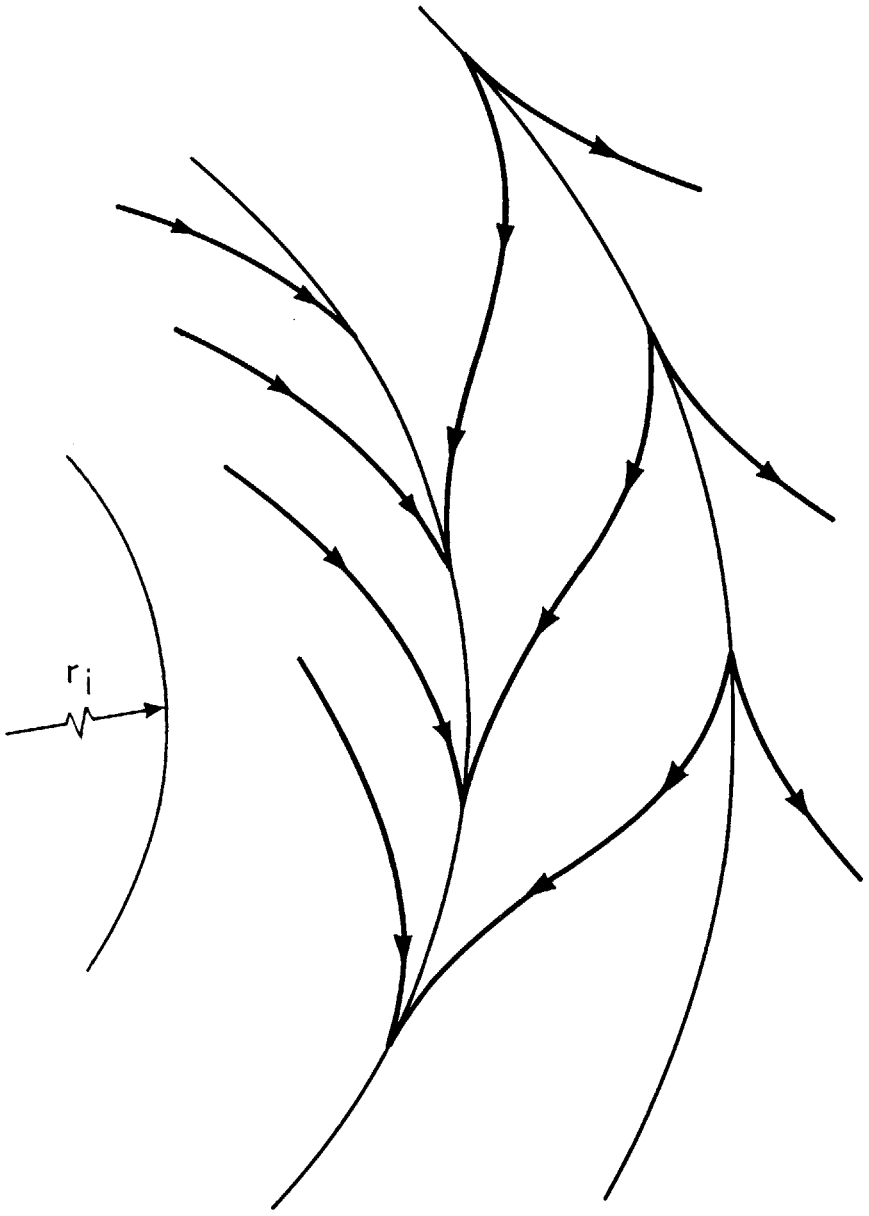

FIGURE 16 - VIEW OF LIMITING WALL STREAMLINES AT SEPARATION BUBBLE.

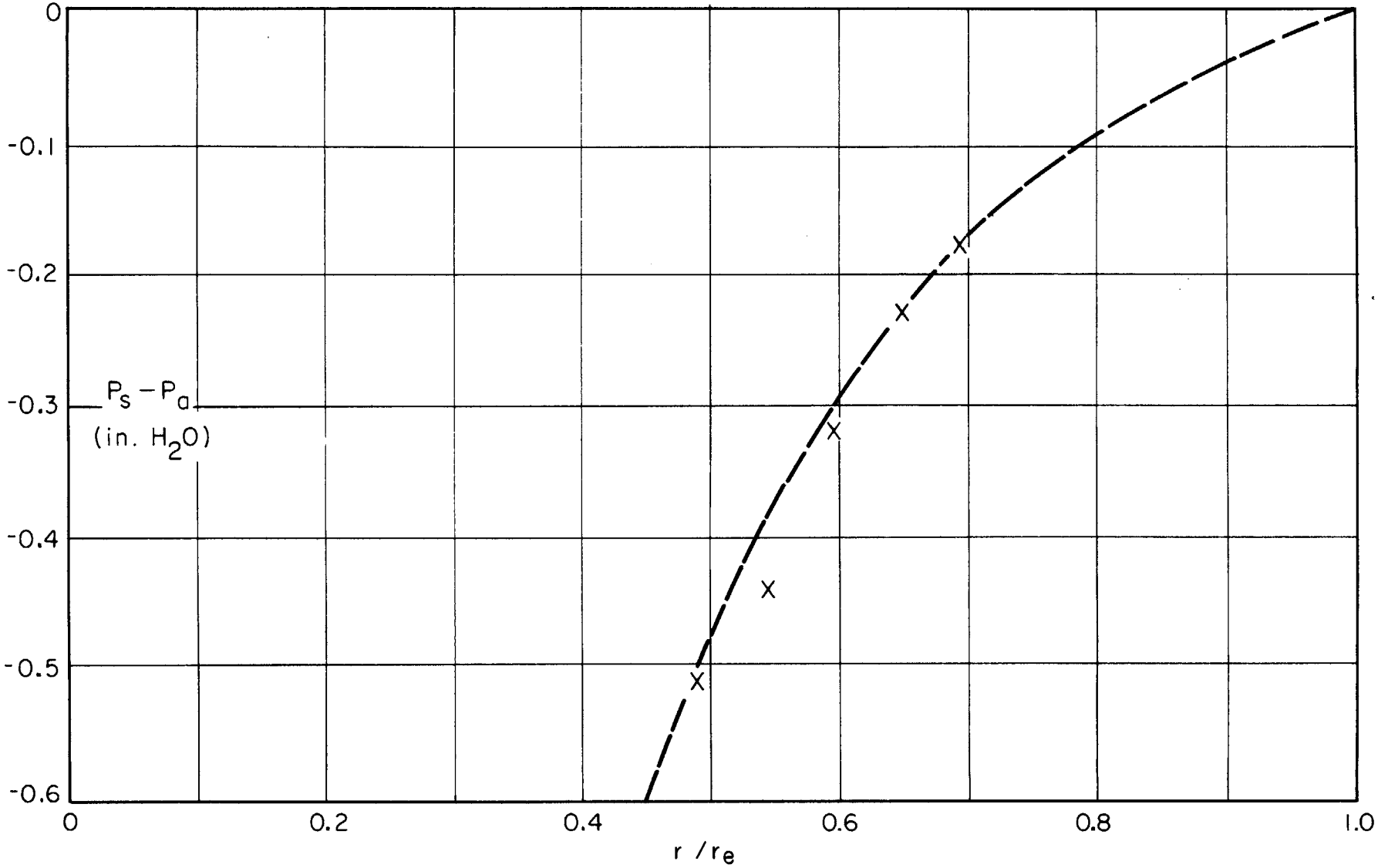

FIGURE 17 - STATIC PRESSURE DISTRIBUTION FOR RUN B-59.6